Impact of flow distortion corrections on turbulent fluxes estimated by the inertial dissipation method during the FETCH experiment on R/V L'Atalante

H. Dupuis, C. Guerin, Danièle Hauser, Alain Weill, P. Nacass, W. M. Drennan, S. Cloché, H. C. Graber

JOURNAL OF GEOPHYSICAL RESEARCH, VOL. 108, NO. C3, 8064, doi:10.1029/2001JC001075, 2003

Impact of flow distortion corrections on turbulent fluxes estimated by the inertial dissipation method during the FETCH experiment on R/V *L'Atalante*

H. Dupuis,[1] C. Guerin,[2] D. Hauser,[2] A. Weill,[2] P. Nacass,[3] W. M. Drennan,[4] S. Cloché,[5] and H. C. Graber[4]

Received 30 July 2001; revised 9 May 2002; accepted 28 May 2002; published 13 March 2003.

[1] The FETCH campaign was for a large part devoted to the measurement and analysis of turbulent fluxes in fetch-limited conditions. Turbulent measurements were performed on board the R/V *L'Atalante*, on an ASIS spar buoy and on aircraft. On the R/V *L'Atalante*, turbulent data were obtained from a sonic anemometer and from a microwave refractometer. The main focus of this paper is to present results of momentum and heat fluxes obtained from the R/V *L'Atalante*, using the inertial-dissipation method and taking into account flow distortion effects. Numerical simulations of airflow distortion caused by the ship structure have been performed to correct the wind measurements on the R/V *L'Atalante* during the FETCH experiment. These simulations include different configurations of inlet velocities and six relative wind directions. The impact of airflow distortion on turbulent flux parameterizations is presented in detail. The results show a very large dependence on azimuth angle. When the ship is heading into the wind (relative wind direction within ±38° of the bow), the airflow distortion leads to an overestimation of the drag coefficient, associated with a wind speed reduction at the sensor location. For relative wind directions of more than ±38° from the bow, flow distortion causes the wind to accelerate at the sensor location, which leads to an underestimate of the drag coefficient. The vertical displacement of the flow streamlines could not be fully established by numerical simulation, but the results are in qualitative agreement with those inferred from the data by prescribing the consistency of momentum flux as a function of azimuth angle. Both show that the vertical elevation of the flow can be considered as constant (1.21 m from numerical simulations) only within about ±20° from bow axis. Values of vertical displacements up to 5 m are found from the data for high wind speeds and beam-on flows. Our study also shows that the relative contributions of the streamline vertical displacement and the mean wind speed underestimate or overestimate vary significantly with relative wind direction. The relative contribution due to vertical streamline displacement is higher for heat flux than for momentum flux. The consistency of our correction for airflow distortion is assessed by the fact that the correction reduces the standard deviation of the drag coefficient: only if this correction is taken into account, do the curves of the drag coefficient versus wind speed become similar for data corresponding to wind in the bow direction and from the side. When the complete numerical airflow correction is applied to the data set limited to relative wind directions at ±30° from the bow axis, the drag coefficient formula is $C_{D10N} \times 1000 = 0.56 + 0.063\ U_{10N}$, for $U_{10N} > 6$ m s^{-1}. This formula provides C_{D10N} values comparable to the ones found from the ASIS buoy data for wind speeds of about 13 m s^{-1}. They are however smaller by 9% at higher winds (>15 m s^{-1}). This formula is also similar, within a few percent, to the parameterizations of *Smith* [1980], *Anderson* [1993], and *Yelland et al.* [1998]. The exchange coefficient for evaporation is found to be 1.00×10^{-3} on average with a small standard deviation of 0.31×10^{-3}. A slight increase of C_{E10N}

[1]Département de Géologie et Océanographie, UMR 58 05, Talence, France.
[2]Centre d'étude des Environnements Terrestre et Planétaires (CETP)/IPSL/CNRS, Vélizy, France.
[3]Meteo-France/CNRM/Centre d'Aviation Meteorologique, Aerodrome, Bretigny-sur-Orge, France.
[4]Rosenstiel School of Marine and Atmospheric Science, University of Miami, Miami, Florida, USA.
[5]Universite Pierre et Marie Curie, IPSL, Paris, France.

0148-0227/03/2001JC001075

value with wind speed is, however, observed with a variation of about 20% (0.2×10^{-3}) for wind speeds between 6 and 17 m s^{-1}, following $C_{E10N} \times 1000 = 0.82 + 0.02\ U_{10n}$, for $U_{10n} > 6$ m s^{-1}. *INDEX TERMS:* 4504 Oceanography: Physical: Air/sea interactions (0312); 4568 Oceanography: Physical: Turbulence, diffusion, and mixing processes; 4594 Oceanography: Physical: Instruments and techniques; *KEYWORDS:* wind stress, heat flux, air-flow over ships, turbulent flux measurements

Citation: Dupuis, H., C. Guerin, D. Hauser, A. Weill, P. Nacass, W. M. Drennan, S. Cloché, and H. C. Graber, Impact of flow distortion corrections on turbulent fluxes estimated by the inertial dissipation method during the FETCH experiment on R/V *L'Atalante*, *J. Geophys. Res.*, *108*(C3), 8064, doi:10.1029/2001JC001075, 2003.

1. Introduction

[2] Many experimental campaigns have been undertaken during the last decades to parameterize turbulent fluxes over the ocean. A good accuracy of these parameterizations is required to reduce uncertainties of the global modeling of the ocean/atmosphere system. Over the ocean, the turbulent fluxes of heat and momentum are estimated using several platforms such as R/Vs of different sizes and shapes, moored buoys or coastal platforms. Concerning the methods, the inertial dissipation method has been used for years [*Large and Pond*, 1981; *Fairall and Larsen*, 1986; *Edson et al.*, 1991]. The main advantage of this method is that it can avoid motion corrections, since measurements are done in the inertial subrange at higher frequencies than those of the platform motion. More recently, technical improvements have allowed the use of the direct method of eddy correlation from ship or buoys [e.g., *Fujitani*, 1981; *Drennan et al.*, 2003; R. Pedreros et al., Momentum and heat fluxes by eddy correlation on R/V *L'Atalante* and ASIS buoy during FETCH experiment, submitted to Journal of Geophysical Research, 2002 (hereinafter referred to as Pedreros et al., submitted manuscript, 2002)] with motion corrections obtained from measurements of a motion package.

[3] It unfortunately appears that the set of bulk coefficients available in the literature presents a significant scatter. Several factors can be invoked to explain this fact. The first is experimental. The effect of flow distortion around measurement platforms has been pointed out as a possible cause for differences between flux estimates from one platform to the other in similar experimental conditions [*Ching*, 1976; *Blanc*, 1986, 1987; *Yelland et al.*, 1998]. Whereas little is known about the distortion of turbulent eddies, the effect of flow distortion on the mean flow is better quantified [*Edson et al.*, 1998; *Oost et al.*, 1994]. For eddy correlation measurements on bulky platforms, it has been suggested that corrections to both the mean flow and turbulence should be carried out. In contrast, the turbulence scales in the inertial sub-range seem to be unaffected by flow distortion, so that flow distortion effects on inertial dissipation fluxes are limited to mean flow distortion. Although the full modeling of turbulent flow around a distorting body is a difficult task, the effects of flow distortion on the mean flow can be accurately estimated, either by numerical simulation [e.g., *Yelland et al.*, 1998, 2002; *Nacass*, 1999] or using small-scale models in wind tunnels [*Butet*, 2001, 2002]. The effect of mean flow distortion can be significant: for example, *Yelland et al.* [1998] attributed air flow distortion as responsible for initial overestimations of their drag coefficients by up to 60%. They therefore strongly recommended corrections of air-sea fluxes for flow distortion, particularly when measured from large structure R/Vs.

[4] A second factor which leads to scatter in the bulk parameterizations is the role of sea state. Surface waves are not passive roughness elements, but interact with the atmosphere. In particular, it is now known that the presence of either strong swell [*Volkov*, 1970; *Donelan et al.*, 1997], or developing wind-waves [see *Kitaigorodskii*, 1970; *Drennan et al.*, 2003] can modify the momentum flux over typical open ocean values. A third factor, related to sea state, is that of nonstationarity of either the wind or wave fields [*Geernaert et al.*, 1986].

[5] To understand the physical coupling between wind and waves, and to progress in the parameterization of the turbulent fluxes, an analysis over a wide range of conditions is needed. These measurements of turbulent fluxes have to be very carefully performed to ensure the validity of the datasets, and to avoid possible discrepancies between methods or platforms.

[6] The FETCH experiment [see also *Hauser et al.*, 2003] took place in March and April 1998 in the North Mediterranean Sea (Gulf of Lion). One of its main objectives was the estimation and parameterization of turbulent fluxes in this coastal area, often dominated by short fetch conditions, due to the frequent occurrence of on-shore winds (Mistral events). Other objectives deal with the wave field evolution, and with remote sensing of the marine atmospheric boundary layer and of the ocean surface [see *Hauser et al.*, 2003].

[7] Concerning the flux measurement and parameterization, the FETCH experiment provides an interesting data set since it includes in situ observations from different platforms. In particular, turbulent flux measurements were performed both on the oceanic R/V *L'Atalante*, which cruised over an area of about 100 km $\times$ 100 km and on an ASIS Spar buoy [*Graber et al.*, 2000] moored in deep water at about 60 km from the shore. In addition to long legs performed by the R/V *L'Atalante* to sample a variety of wind/wave conditions, several periods of observations with the R/V in the vicinity of the buoy were organized with the aim of comparing turbulent fluxes estimated from different platforms and methods.

[8] The general meteorological and oceanic conditions during FETCH are described by *Hauser et al.* [2003] and summarized hereafter. Wind speeds range from about 1 m s^{-1} to 19 m s^{-1}. Stratification conditions are mainly unstable, except in light wind conditions (less than about 5 m s^{-1}). Wave conditions include wind-sea cases with

inverse wave age, defined as u^*/C_p, (where u^* is the friction velocity and C_p the phase speed of the dominant waves), from 0.03 to 0.1, as well as mixed sea cases and swell cases.

[9] In this study, we focus on the impact of distortion of the mean flow on turbulent fluxes calculated by the inertial dissipation method. This effect on measurements from large R/V must be fully discussed before the influence of sea state can be analyzed. A thorough study on the impact of airflow distortion indeed appeared necessary because preliminary results from the R/V *L'Atalante* data during FETCH, without accounting for flow distortion, showed C_{D10N} values significantly in excess compared to measurements of the ASIS buoy [*Dupuis et al.*, 1999; *Hauser et al.*, 2000]. In this paper, the sensitivity of the drag and heat exchange coefficients to the corrections for airflow distortion is evaluated. These corrections are based on 3D numerical simulations of flow distortion around the R/V *L'Atalante*, including the instrumented mast deployed on the foredeck during the FETCH experiment. Drag and exchange coefficients for heat and evaporation are compared using a full correction, a simplified correction or no correction. Results from the R/V *L'Atalante* by the inertial dissipation method and accounting for a correction of airflow distortion are then compared to those of the ASIS buoy, calculated by the eddy correlation method, to evaluate the consistency of the dataset. A further comparative analysis including eddy correlation results on R/V *L'Atalante* is presented by Pedreros et al. (submitted manuscript, 2002).

[10] We first describe in section 2 the experimental setup used on the R/V *L'Atalante* during FETCH for turbulent fluxes. Then, in section 3, the main results obtained from the airflow numerical simulations are presented. Sections 4 and 5 summarize the method used to estimate the fluxes, and to account for the flow distortion in the estimates. Section 6 presents the analysis of the vertical displacement due to air flow distortion and results for the drag and exchange coefficients with different conditions for flow distortion correction: no correction, complete correction (horizontal relative wind speed and direction, plus vertical displacement corrections as a function of relative wind direction), partial correction (horizontal wind speed and direction correction function of the relative wind direction, and no vertical displacement), and simplified correction (constant horizontal wind speed and vertical displacement correction). The consistency of the complete correction is evaluated by comparing C_{D10N} values for different ranges of relative wind direction. As a second validation, wind speeds and friction velocities are compared to those of the ASIS buoy for different ranges of separation distances. Then, the effect of the different corrections is analyzed. Finally, parameterizations are proposed for the FETCH turbulent fluxes estimated by the inertial dissipation method on R/V *L'Atalante* and compared to those of the ASIS buoy during FETCH and to other studies.

2. Experimental Setup

2.1. Shipborne Measurements

[11] During FETCH, the R/V *L'Atalante* was equipped with sensors to investigate air-sea interactions and particularly sensors devoted to the measurements of turbulent fluxes of heat and momentum. The present study is based on the data from several turbulent meteorological sensors. A Gill ultra sonic anemometer (R3 research HS, from Gill Instruments Ltd) is used to provide the three components of wind velocity, along with sonic temperature. In addition, a microwave refractometer, based on a resonant microwave cavity, is used to provide the fluctuations of the air refraction index. This device combines a circular cylindrical "open" cavity made of Zerodur-M glass ceramics from SCHOTT operating near 9.4 GHz with a frequency measurement system. The determination of the resonant frequency is related with the air (filling the cavity) refraction index. Sonic anemometer and refractometer are synchronized and work with a sampling rate of 50 Hz. A full description of the refractometer, designed at CETP, is given by *Delahaye and Fournet-Fayas* [1988] and *Delahaye et al.* [2001]. This sensor provides very reliable measurements [*Dupuis et al.*, 1999; *Eymard et al.*, 1999] for humidity fluctuations as demonstrated by Figure 11 of *Delahaye et al.* [2001] showing normalized spectra of air refraction index as a function of frequency and wavelength for a large range of wind speed and stratification. In contrast, reliable measurements of temperature fluctuations are very difficult to obtain over the ocean, mostly due to salt contamination on sensors. Both sonic temperature and air refraction index depend on air temperature and humidity. Hence, both the latent and sensible heat fluxes can be derived (see section 4 below). Although the sonic thermometer is a promising technique to estimate the sensible heat flux (because it is not affected by salt contamination), especially when the data are analyzed with the eddy correlation method (Pedreros et al., submitted manuscript, 2002), we confirm here that it still needs improvements to accurately estimate sensible heat flux when the inertial dissipation method is applied [see also *Larsen et al.*, 1993; *Dupuis et al.*, 1999; *Eymard et al.*, 1999]. This is due to the poor accuracy of the sonic temperature measurements at the high frequencies needed for the inertial dissipation method. Hence, only an order of magnitude of the sensible heat flux is provided here while momentum and latent heat flux estimates are of better quality.

[12] The turbulence sensors were located at about 17.8 m, at the top of a foredeck mast (see Figure 1a). Figure 1 of Pedreros et al. (submitted manuscript, 2002) also provides a detailed sketch of the experimental set-up on the mast. In addition to observations from the turbulent sensors, data from the following instruments are used in the present study. Meteorological sensors (humidity and temperature transmitter HMP233 manufactured by Vaisala Oy., PTB220 barometer) are used to provide mean parameters such as air temperature, humidity and pressure. GPS and navigation data from the vessel are used to transform the wind measurements to the earth reference frame. Additional shipborne measurements include: currents by Acoustic Doppler Profilers (ADCP); wave conditions by video and photo-stereogrammetry; and oceanic and atmospheric profiles by CTD and radio soundings respectively. It is worthwhile noting that the surface currents as measured by shipboard ADCP are negligible in the wind direction and are thus not accounted for. Indeed, at meso-scale, currents are parallel to the coast. The order of magnitude of currents at the level nearest to the surface (in 10 m depth) is of 20 or

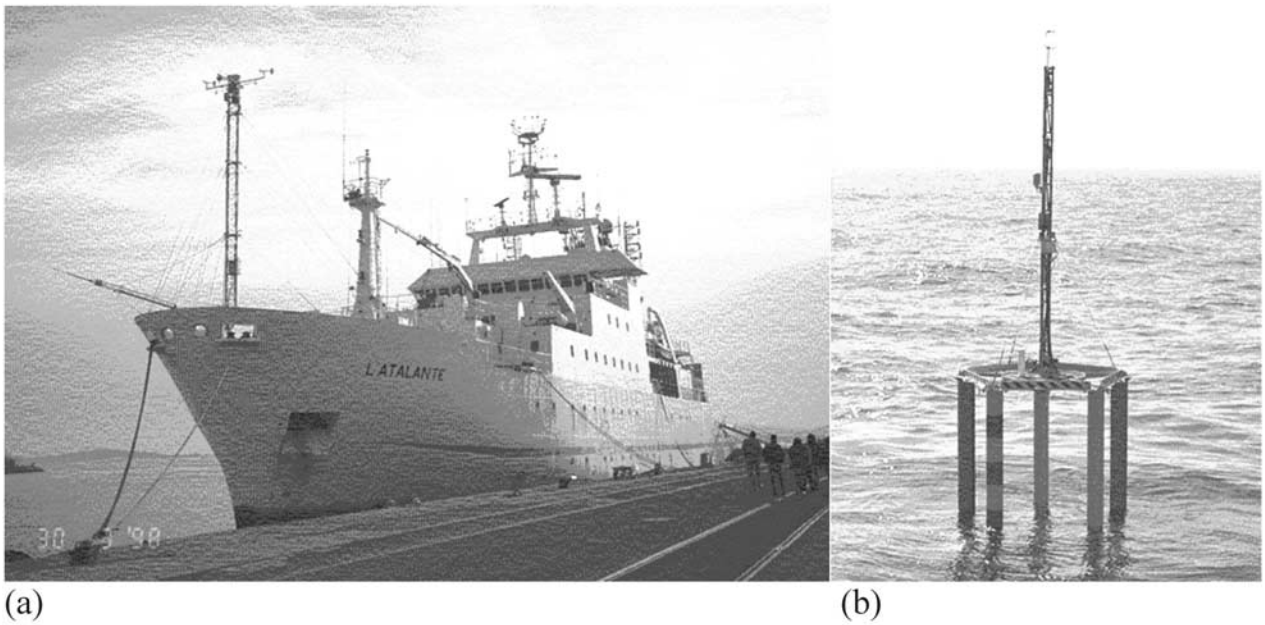

Figure 1. Photographs of (a) the R/V *L'Atalante* and (b) the ASIS buoy during the FETCH experiment.

30 cm s^{-1} after the highest wind events (in these cases the wind blew perpendicular to the coast).

2.2. ASIS Buoy Measurements

[13] For comparison with the R/V *L'Atalante* data, data from an ASIS (Air-Sea Interaction Spar) buoy are used. ASIS buoys were designed specifically for research at the air-sea [*Graber et al.*, 2000]. The buoys are constructed using an open structure (see Figure 1b), and hence cause very little flow distortion to the wind field. The largest structural elements above the surface are 20 cm diameter cylinders, and these terminate 4 m below the anemometer. The mast itself is an open triangular pylon constructed with 3.5 cm (max) diameter members. Although flow distortion studies have not yet been carried out for ASIS, such effects are expected to be very small.

[14] The ASIS buoy was moored at 42°58′56″ N, 04°15′11″ E, roughly 50 km SSW of the Rhone delta. The fluxes are calculated using the eddy correlation method, with data from a Gill R2A sonic anemometer located 7 m above mean sea level. The full motion of the buoy is measured, and these motion signals are used to correct the measured velocities prior to calculating the fluxes (see *Drennan et al.* [2003] for details). When comparing the *L'Atalante* and ASIS fluxes, we restrict our attention to periods when the ship is located close to ASIS, thus ensuring that the two platforms are in similar sea states. In general, this is not the case, and quite often the ship and buoy are experiencing quite different sea state conditions. See *Drennan et al.* [2003] for a discussion of the effect of wave development (wave age) on momentum flux.

3. Airflow Simulation

[15] The distortion of the air flow caused by the ship and its hull, the decks and the instrumented mast was simulated in three dimensions by computational fluid dynamics software. The numerical model, which is based on a finite volume method, is suited for incompressible and compressible fluid flow in complex geometries and can be run with several turbulence models such as the standard k-ε or large eddy simulation.

[16] The simulations were run with the Fluent 5 numerical model, commercially available from Fluent Inc.. To use this code, the chosen body must be paneled. The preprocessor available in the same package, is used to compute the geometry modeling and the mesh generation. It allows structured, unstructured and mixed meshes.

[17] The R/V *L'Atalante* is 85 m long from stem to stern and 16 m wide. Its height is 18 m above the sea level at the summit of the mast. The mast is located on the centerline of the ship, about 2 m behind the stem. The turbulent sensors are located at the top of the mast (refractometer) and at the end of a 1 m boom in front of the upper part of the mast (sonic anemometer). The latter point is the reference taken in this study for airflow distortion correction. In the numerical model, the ship body is enclosed in a large rectangular volume of 195 m long, 60 m wide and 60 m high above the sea level to simulate a wind tunnel. Considering R/V's projected surface areas of 223 m^2 and 759 m^2 respectively in the front and port (or starboard) directions, a blocking ratio of 0.06 is obtained in both cases [*Castro and Robins*, 1977]. Therefore, due to the finite dimension of the wind tunnel in the simulations, the maximum error can be as high as 6% for the horizontal wind speed magnitude, particularly at the navigation bridge. However, the projected surface area of the foredeck is much smaller and a maximum error due to the blockage of 1% is more realistic at the sonic location. This is supported by the good agreement between numerical simulation and the physical simulations of *Butet* [2002] who used a maximum blocking ratio of 0.024. These are described below. Hence, although the conditions of simulation are not completely optimal (the flow might be slightly accelerated in the wind tunnel simulations), it is

likely that the error is less than 1% and of the same order for bow and port-starboard directions, due to the same blocking ratio in both directions.

[18] For the ship body and sea surface, the panels are generated as an unstructured mesh of triangular cells, allowing the model to have a fine resolution near the sea surface and the ship body. The boundary sides of the measurement volume are paneled with a structured mesh of rectangular cells. The vertical profile of the inlet wind speed may be adjusted with the vertical distribution of the mesh. The volume is meshed by 90000 hybrid cells composed with 186000 faces. Three dimensional cells in the shape of pyramids and prisms are needed to link the tetrahedral cells (adjacent to the ship body and sea surface) and the hexahedral cells (adjacent to the boundary sides). The model uses a finer resolution of 450 mm for the side of the tetrahedral cells near the instrumented mast. The distance between the sensor and the center of gravity of its corresponding cell is less than 5 mm. However, due to the large difference between the dimensions of the ship hull and of the rungs of the mast lattice, the mast was represented as a full volume of equal size. The validity of this simplification was examined by *Butet* [2002], who carried out physical simulations with the detailed mast. It was shown that considering a solid mast remains appropriate for sensors located within 2 m of the top of the mast (as is the case for the turbulent sensors here) because of the presence of electronic boxes at the top of the mast (Figure 1).

[19] The numerical model also takes into account the thermodynamic characteristics of the sea surface and the material of the ship. Because the processing time to reach convergence is too long with the turbulent flow model, most of the simulations were run in laminar flow conditions. Results obtained in both laminar and k-ε turbulent flow conditions show that considering a laminar flow instead of a turbulent one does not change significantly the results at the sensor location.

[20] The evaluation of the mean airflow vertical displacement was difficult due to the grid configuration. It has however been estimated for wind speeds of 10 m s^{-1} and relative wind directions of 0, 20, 50 and 90° by visual observation of the path line of mass-less particles on outputs of the numerical simulations. The free streamflow is obtained at the inlet of the tunnel. A mean upward streamline displacement of 1.21 m was found at bow angles, while values of about 2.5 m were obtained for other wind directions as shown in Table 1. Note that due to the simulation configuration, the horizontal distance of the streamline between its origin at an inlet wall and the sensors varied from 30 to 66 m depending on the azimuth angle of the wind (see Table 1). *Butet* [2002] obtains a similar value of +1.10 m for bow-on flows. Furthermore, the +1.21 m vertical displacement obtained at bow angles seems reasonable compared to other studies with foredeck masts [*Yelland et al.*, 1998; *Butet*, 2001]. Indeed, these authors find a value of 1 ± 0.3 m for anemometers on masts near the bow of 5 other ships, while greater values of up to 1.5 or 2 m are found for anemometers on a ship's main mast above the accommodation block. Therefore a good confidence is obtained for the value for the vertical elevation for bow-on flows. In contrast, for beam-on flows, there is an underestimation of the vertical elevation of the order of 1 to 2 m.

Table 1. Vertical Displacement in Meters as Obtained by Reversed Path Line in the Numerical Simulations for Upstream Wind Velocity of 10 m s^{-1} and Four Azimuth Angles[a]

Wind Speed ϕ_u	Distance, m	Δz, m
10 m s^{-1}, 0°	62	1.21
10 m s^{-1}, 20°	66	2.43
10 m s^{-1}, 50°	39	2.12
10 m s^{-1}, 90°	30	2.79

[a]The distance to which the reversed path line is followed between the sensor and the "upstream" source location is indicated in second column.

Similar results were found by *Yelland et al.* [2002] in their simulations of the R/V *James Clark Ross*, a vessel similar to *L'Atalante* (see their Figure 13). A complete discussion of the vertical elevation of the flow, including the functions deduced from the data set, can be found in section 6.1. Indeed, we shall thereafter consider two functions for the vertical elevation. First a constant value of 1.21 m, and second a function of both azimuth angle and wind speed as derived from the FETCH data. As shown in section 6.1, the latter function, defined to minimize the flux dependence on azimuth angle, is in qualitative agreement with the initial numerical simulations, which are however found to be underestimated at beam-on flows due to the too small distance of the inlet of the tunnel as suggested by *Yelland et al.*'s [2002] simulations.

[21] For the simulations, wind direction and velocity were specified in a large range of values, with four different (upstream) velocities (5, 10, 15 and 20 m s^{-1}) and six different inlet azimuth angles (0°, 20°, 50°, 90°, 150°, and 180°) with respect to the ship axis. It is assumed that the results are the same for port-side flows as for starboard flows since the mast is on the centerline of the ship (*Butet* [2002], however, identified a small asymmetry due to the ship superstructure). Other calculations have been performed to simulate the effect of swell with the ship in the trough and on the top of a wave. Preliminary simulations have been carried out with the domain tilted in order consider "stationary" effects of roll and pitch [see *Nacass*, 1999]. The results suggest that the mean wind speed error for two opposite tilts is not the same as the error without a tilt.

[22] Validation of the simulations is discussed by comparing the simulated and measured slope angles at the anemometer location over 30 min (Figure 2). The slope angle β is defined as $\beta = \tan(W/U)^{-1}$, where W and U are the simulated or measured mean vertical and horizontal wind speeds at the sonic anemometer location. As Figure 2 shows, a good agreement is obtained between simulated (crosses and line) and observed (dots) values of β, for the six azimuth angles. Indeed, much of the scatter in the data can be attributed to effects not taken into account in the simulations (variation of relative wind magnitude and direction within the time interval, turbulent flow distortion due to the waves). For relative wind directions (or azimuth angles) within ±100° from the bow axis, the slope angles are found to be about 7° both for data and simulations (simulations show a slight decrease of 1° when the absolute relative wind direction is varied from 0 to 100°). Also, the variations at larger azimuth angles are consistent between simulations and observations. The results obtained in a wind tunnel by *Butet* [2002] are also consistent since they provide a slope angle of 6° at similar bow angles at the sensor

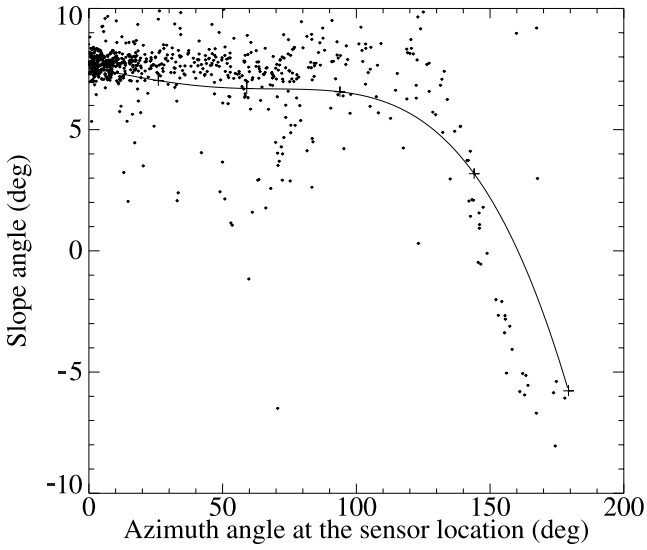

Figure 2. Slope angle β (in degrees) as a function of the relative wind direction (or azimuth angle). Dots, observed slope angles; pluses, slope angles obtained from the numerical simulation of airflow distortion; solid line, fourth-order polynomial fit to the model results.

location. In contrast, previous simulations in which the instrumented mast was not included did not show this agreement: the simulated slope angle for low relative wind directions was found to be about 3° [*Nacass*, 1999]. This indicates that the mast itself plays a major role in the airflow disturbances, even for a large R/V such as *L'Atalante*. More precisely, physical simulations performed in the wind tunnel with a realistic mast [*Butet*, 2002, Figure 10], confirmed that the major disturbance to the flow is caused by the electronic boxes at the top of mast. Indeed, vertical profiles of the slope angle at the sonic anemometer location show that the perturbation has (1) a general feature: a decrease of the slope angle from 3.2 to 2.3° for heights varying from −5 to +5 m relative to the top of the mast and (2) a superimposed local feature limited −2 to +2 m relative to the top of the mast, associated with a maximum of the slope angle of 6° at the top of the mast. This fact seems to be of considerable importance and should be better taken into account in the placement of sensors on meteorological masts for future experimental work. It also implies that simulations have to be redone if another sensor/mast configuration is used on the same R/V.

[23] Simulation results showing the perturbation of the horizontal wind speed relative to the ship due to airflow distortion are presented in Figure 3. Figure 3a shows the relative perturbation of the horizontal wind, in percentage of wind speed, only as a function of azimuth angles and for different wind speeds. The relative wind speed error appears to be independent of the wind speed since data from all wind speeds have been collapsed on a single curve. In contrast, *Yelland et al.* [1998] showed that the wind speed error (and the vertical displacement) both vary slightly with wind speed. A large dependence of the wind speed error is observed with azimuth angle: this error is about −6% (underestimate of the wind speed at the sonic location) when the bow points into the wind, tends to 0 at angles close to ±38° from the bow axis and becomes positive (overestimate of the wind speed) above that angle, up to 20% at 100°. Similar values within 1% were obtained by *Butet* [2002] for azimuth angles limited to 30° (−7% at bow angles for example). Figure 3b shows that the wind direction is also affected by airflow distortion, with errors up to 10° at 50° azimuth angle. Fifth- and fourth-order polynomial fits obtained from these simulations are indicated respectively in Figures 3a and 3b as solid lines. They can be expressed as:

$$\frac{U_s - U_u}{U_u} \times 100 = -5.76 - 0.192\phi_s + 0.015\phi_s^2 - 1.39e-4\phi_s^3 + 3.51e-7\phi_s^4 - 1.43e-10\phi_s^5 \quad (1)$$

$$\phi_u = -0.2056 + 0.7283\phi_s + 8.626e-4\phi_s^2 + 3.130e-5\phi_s^3 - 1.534e-7\phi_s^4, \quad (2)$$

where subscript *u* stands for the upstream value (value which would be observed in absence of flow distortion) and

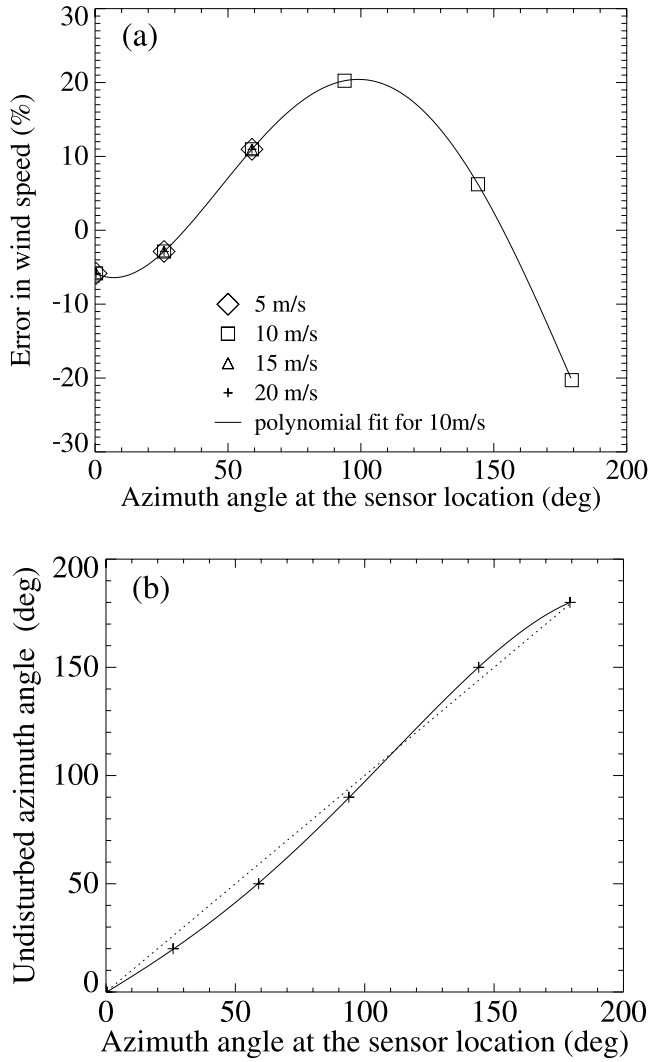

Figure 3. Results from the numerical simulation of flow distortion. (a) Horizontal relative wind speed error (in %) due to air flow distortion as a function of the measured azimuth. (b) Deviation of the relative wind direction (or azimuth angle) due to flow distortion.

subscript *s* for the value at the sensor location with flow distortion.

[24] Figure 4 shows the comparison of the uncorrected versus corrected relative wind speeds for the whole data set on R/V *L'Atalante* during FETCH (averaging time of 30 min). The corrected values are calculated by using equation (1). The scatter diagram is split in two parts, with positive (respectively negative) corrections of the horizontal relative wind speeds for absolute values of the apparent wind direction smaller (respectively larger) than 38°. Maximum corrections reach about 2.5 m s^{-1} at high wind speed (above 25 m s^{-1}, in the ship reference frame) and for relative wind directions higher in magnitude than 38°. Due to the larger number of data points at small relative wind directions in the data set (i.e., 80% of the data correspond to absolute values of relative wind directions less than 20° from the bow axis), the corrected wind speeds are higher on average than the measured ones.

[25] Before we show how these corrections are introduced in the flux calculations and how they affect flux parameterizations, the derivation of the turbulent fluxes is reviewed in the next Section.

4. Flux Derivations

[26] The dissipation method has been used for 30 years over the ocean. The method was reviewed by *Fairall and Larsen* [1986] and *Edson et al.* [1991]. These latter authors, as well as *Large and Pond* [1981] and *Smith et al.* [1992], have also contributed to the validation of the method by comparison of the results with those by eddy correlation. In this study, the method to derive the turbulent fluxes of momentum, sensible and latent heat is quite similar to what is presented by *Dupuis et al.* [1999]. For FETCH, dissipation rates are calculated every 30 min from the density spectra of the along-wind wind component, sonic temperature, and refractive index. A minimum frequency range of 2 Hz is selected to estimate the dissipation rates within the inertial sub-range by using:

$$\varepsilon_u = (L_u/\alpha_u)^{3/2}(2\pi/U_r) \tag{3}$$

$$\varepsilon_{t_s} = (L_{t_s}/\alpha_{t_s})\varepsilon^{1/3}(2\pi/U_r)^{2/3} \tag{4}$$

$$\varepsilon_n = (L_n/\alpha_n)\varepsilon^{1/3}(2\pi/U_r)^{2/3}, \tag{5}$$

where subscripts u, t_s, and n refer to the along-wind wind component, the sonic temperature, and the refractive index, respectively. L_i, for each of these variables (subscript i stands for u, t_s or n), is the mean spectral energy multiplied by $f^{5/3}$ where f is the frequency, and α_i are universal constants. The experimental values of the Kolmogorov constant, $\alpha_u = 0.55$, and of the Obukhov-Corrsin constant, $\alpha_{ts,n} = 0.8$ are used respectively in equations (3)–(5). U_r is the relative wind speed.

[27] Derivation of the fluxes using the Turbulent Kinetic Energy (TKE) and scalar variance budgets is based on the following equations (6)–(9), and has been described in detail by *Dupuis et al.* [1997, 1999]. Kinematic vertical fluxes $\langle uw\rangle$, $\langle wt_s\rangle$ and $\langle wn\rangle$ (defined with brackets indicating time averaging of lower case variables as turbulent quantities) are estimated through:

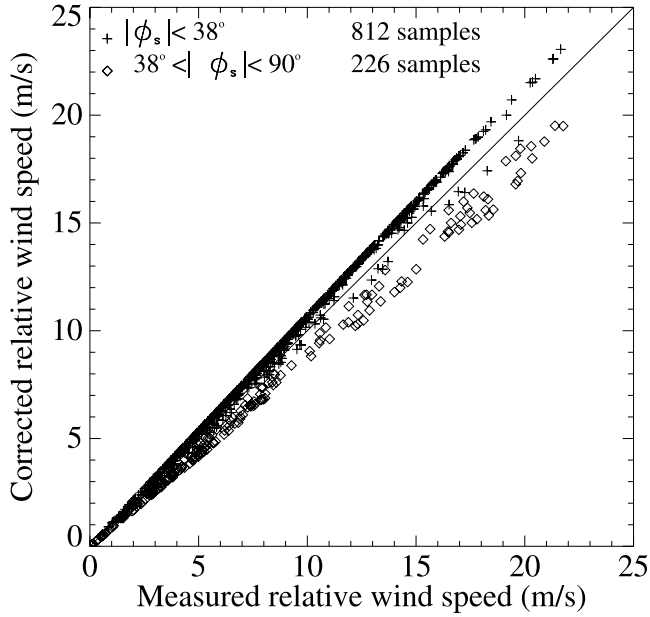

Figure 4. Scatterplot of corrected versus uncorrected horizontal relative wind speed. The corrected wind speed was obtained through equation (1). Pluses, samples for absolute azimuth angles less than 38° (812 samples); diamonds, samples for absolute angles between 38 and 90° (226 samples).

$$u^* = [\kappa Z \varepsilon_u/(\Phi_m(Z/L) - Z/L - \Phi_{imb}(Z/L))]^{1/3} \tag{6}$$

$$\langle wt_s\rangle = [\kappa Z u^* \varepsilon_{t_s}/\Phi t_s(Z/L)]^{1/2} \tag{7}$$

$$\langle wn\rangle = [\kappa Z u^* \varepsilon_n/\Phi_n(Z/L)]^{1/2} \tag{8}$$

$$L = -T_v u^{*3}/(g\kappa\langle wt_v\rangle), \tag{9}$$

where Z is the height of measurement above the sea surface, $u^* = \langle -uw\rangle^{1/2}$ is the friction velocity, T_v is the virtual temperature, κ is the Von Karman constant (0.4), L is the Monin Obukhov (MO) Length, estimated using the bulk parameterization as defined in section 5, and the stratification functions (Φ_m, Φ_{ts}, Φ_n) are estimated according to *Large and Pond* [1982].

[28] In equation (6), $\Phi_{imb}(Z/L)$ is an empirical imbalance function of the TKE budget [e.g., *Wyngaard and Coté*, 1971; *Yelland and Taylor*, 1996; *Janssen*, 1999; *Taylor and Yelland*, 2000]. *Dupuis et al.* [1997] found that it was necessary to introduce this stability dependent imbalance term in order to minimize the dependence on stability of the drag coefficient over the ocean calculated by the inertial dissipation method. Further analysis applied to 4 experiments including very different stratifications [*Eymard et al.*, 1999] corroborate this stability dependent imbalance term.

This term was estimated as $-0.5Z/L$. It is used with the same parameterization in the present study. We note that, as shown by *Dupuis et al.* [1999], the FETCH experiment did not encounter extreme stratifications, so that except for a few samples, the impact of this imbalance term on the C_{D10N} values from FETCH is much less than 1%.

[29] The sensible and latent heat fluxes are calculated by using a decomposition of the terms $\langle wt_s \rangle$ and $\langle wn \rangle$ of equations (7)–(8) as linear functions of the more classical vertical kinematic fluxes of humidity $\langle wq \rangle$ and dry air temperature $\langle wt \rangle$:

$$\langle wt_s \rangle = \partial T_s/\partial T \langle wt \rangle + \partial T_s/\partial Q \langle wq \rangle \tag{10}$$

$$\langle wn \rangle = \partial N/\partial Q \langle wq \rangle + \partial N/\partial T \langle wt \rangle, \tag{11}$$

where $\partial T_s/\partial T$ and $\partial T_s/\partial Q$ are the partial derivative of mean parameters T_s with respect to air temperature T and specific humidity Q, respectively. They can be expressed as $(1 + 0.518Q)$ and $0.518T$, respectively where Q and T are the mean values for q and t. Indeed:

$$N = P\left(77.6/T + 3.73\ 10^5 Q/0.622T^2\right) \tag{12}$$

$$T_s = T(1 + 0.518Q), \tag{13}$$

From these expressions, it can be verified that the flux of the air refraction index, $\langle wn \rangle$, depends mainly on $\langle wq \rangle$, for typical Bowen Ratios over the sea. This is because $\partial N/\partial Q$ is one order of magnitude larger than $\partial N/\partial T$ (with opposite sign). The partial derivative of the mean air pressure P is neglected because it is a third order term. This is discussed in detail, with Bowen ratios typical for the FETCH experiment, by *Delahaye et al.* [2001]. A bulk estimate of $\langle wt \rangle$ is used to estimate $\langle wq \rangle$ from equation (11). Although the system of equations (10)–(11) could have been solved for both $\langle wt \rangle$ and $\langle wq \rangle$, it was not done, because the poor quality of $\langle wt_s \rangle$ estimated from the sonic temperature would have added significant noise in the latent heat flux estimates. In contrast, the fluctuations of the air refraction index are of good quality (again, see Figure 11 of *Delahaye et al.* [2001]).

[30] The main changes concerning the processing compared to these previous publications are the following. (1) The frequency range of the inertial sub-range is adapted at each sample, using a criteria based on the goodness fit of a $-5/3$ power law. Typically, this inertial subrange is at least 2 Hz wide. (2) the dissipation rates are computed every 30 min of observations, using at least 120 independent averaged spectra of 512 samples each (10.24 seconds long), thus covering a minimum of 20.48 min of data. This allows more samples to be considered than using a single spectra over 30 min. (3) The wind speed used in the bulk formulae is taken from the sonic measurements instead of from the measurements of the YOUNG propeller has it was previously. This ensures a consistency in the corrections for flow distortion, which has been estimated at the sonic sensor location. (4) Data were rejected if the range of relative wind direction exceeds ±100 (instead of ±50) degrees from the bow axis. This wider azimuth range allows us to analyze the impact of wind azimuth on the flow distortion corrections.

5. Method of Flux Corrections

[31] The corrections are based on the assumption that only the mean characteristics of the wind speed are disturbed by the R/V, while the turbulence in the inertial sub-range is not affected. Thus the turbulent fluxes are corrected as follows. (1) Dissipation rates are calculated with equations (3)–(5) using the measured uncorrected values for the mean relative wind speed, U_r and the spectral densities (indeed, the relative wind speed is used here to transform frequency in wave number following the Taylor hypothesis and it should not be corrected). (2) The relative wind speed averaged over 30 min is corrected for air flow distortion using equations (1)–(2). The wind speed in the earth reference frame is then calculated from this corrected relative wind speed. (3) The measurement height Z is corrected for vertical displacement which is fixed at a value of 1.21 m, hereafter denoted with subscript CVE, at a first step (section 6.1) and then computed using equation (18) (section 6.2 and in the following), hereafter denoted the "complete flow distortion correction". (4) Bulk formulae are used to derive the MO length L (equation (9)): the parameterization of *Smith* [1980] is used for the neutral drag coefficient in the momentum flux; for the heat fluxes we use transfer coefficients of 1.2×10^{-3} at unstable stratification and 0.7×10^{-3} at stable stratification (only for the sensible heat flux). These values are consistent with most experimental studies [*Large and Pond*, 1982; *DeCosmo et al.*, 1996; *Smith*, 1988]; see *Fairall et al.* [1996] for a detailed description of bulk parameterizations. (5) Equations (6)–(11) are solved using sensor elevations corrected for the vertical displacement. (6) Drag and exchange coefficients for latent and sensible heat fluxes (C_{D10N}, C_{E10N} and C_{H10N}) are derived using the 10 m equivalent neutral parameters noted "10N" and using the corrected wind speed in the earth reference frame:

$$C_{D10N} = \frac{u^{*2}}{U_{10N}{}^2} \tag{14}$$

$$C_{E10N} = \frac{\langle wq \rangle}{U_{10N}(Q_{sat} - Q_{10N})} \tag{15}$$

$$C_{H10N} = \frac{\langle wt \rangle}{U_{10N}(SST - T_{10N})}, \tag{16}$$

where U, SST and Q_{sat} stand respectively for mean values of wind speed, sea surface temperature and humidity at saturation (a coefficient of 0.98 is used in the calculation of Q_{sat} for the salt water correction).

6. Results

6.1. Estimation of the Vertical Elevation by Prescribing a Consistency of Momentum Flux as a Function of Azimuth Angles

[32] Consistency of the airflow correction provided by the "Fluent" simulations (so-called "CVE") is assessed by the

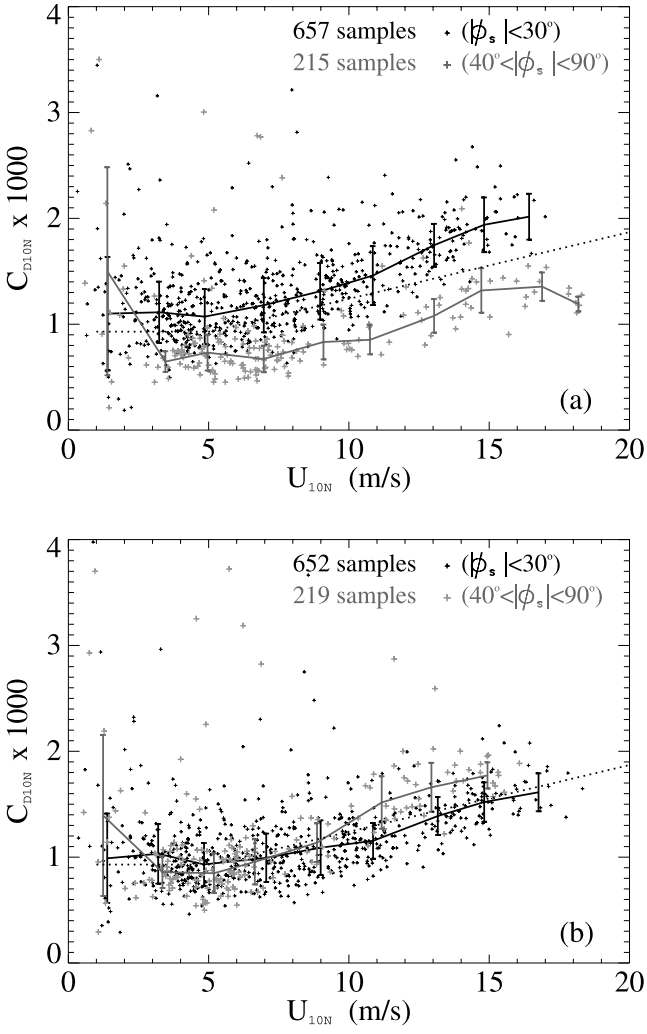

Figure 5. C_{D10N} values versus U_{10N} obtained from the R/V *L'Atalante* measurements with the inertial dissipation method (a) without correction for airflow distortion and (b) with "CVE" correction for airflow distortion. In each plot, two ranges of absolute values of the azimuth angles are distinguished: within ±30° of the bow (solid pluses and solid lines in black) and from the port or starboard directions (between ±40 and ±90° of the bow, shaded pluses and solid shaded lines). Solid lines join the mean values of C_{D10N} calculated in classes of 2 m s^{-1} bins. Error bars indicate the standard deviation with respect to the mean in each wind speed bin. The dotted line is the parameterization of *Smith* [1980]. The number of samples in each bin of wind direction changes when the flow distortion correction is applied, following equation (2).

analysis of the drag coefficients. We focus on the drag coefficient here, because the impact of the correction is more significant than for the heat coefficients (the wind speed is squared in equation (14) in contrast with heat flux equations, equations (15)–(16)). Parameterizations for heat fluxes will however be discussed in the next sections.

[33] Due to the opposite effect of the flow distortion on the mean wind speed for absolute azimuth angles less than and larger than about 38°, the data set has been separated in two subsets, one with absolute azimuth angles less than 30°, and the other ranging between 40° and 90°. Figure 5 shows the C_{D10N} values in these two classes of azimuth angles. The Figure 5a displays the drag coefficients with no flow distortion correction, showing a factor of nearly 2 for C_{D10N} between the two classes at moderate wind speeds (data within ±30° from the bow axis are larger than data corresponding to wind angles from port or starboard). Differences in C_{D10N} values increase with wind speed. When the correction with constant vertical elevation is applied as explained in section 5, the two subsets agree remarkably well for wind speeds below 10 m s^{-1} (Figure 5b). Above 10 m s^{-1}, C_{D10N} values for those data with wind direction from port or starboard are somewhat larger than those for data with wind directions within ±30° of the bow. Thus the FETCH data indicate that if a constant vertical elevation is suitable at a low to moderate wind speed regime (<10 m s^{-1}), a more sophisticated vertical elevation has to be considered at higher winds.

[34] In the following it is supposed that the only source of inconsistency in relative wind direction that remains in the FETCH data is due to the constant vertical elevation used in the airflow distortion correction.

[35] To determine the variation of the vertical streamline elevation with both relative wind direction and wind speed, data corrected for air flow distortion are used with the correction of the mean wind (error in magnitude and direction) and with the constant vertical elevation of 1.21 m (CVE).

[36] Equation (6) implies that if we have knowledge of the true value of the friction velocity, u^*_{true}, and the estimated value u^*_{CVE} obtained by IDM using air flow distortion correction with constant vertical elevation with altitude Z_{CVE}, then:

$$u^*_{CVE}/u^*_{true} = (Z_{CVE}/Z_{true})^{1/3} \qquad (17)$$

provided stratification is near neutral.

[37] Bow-on flow ($|\phi| < 10°$) samples are used to determine u^*_{true} by interpolation based on mean friction velocities in 2 m s^{-1} wind speed bins. Figure 6 shows the ratio u^*_{CVE}/u^*_{true} as a function of absolute value of relative wind direction (in 10° direction bins) as error plots with the mean values and standard errors of the ratio. The range of Z over L used in Figure 6 is −0.5 to 0.2 which corresponds to 770 samples. Figure 6 shows that the ratio depends not only on relative wind direction, but also on wind speed as suggested by Figure 5. Indeed, the two error plots correspond to relative wind speeds smaller or greater than 10 m s^{-1}, respectively for diamond and plus symbols. Figure 6 shows ratio of about 1.09 for relative wind directions above 30° and relative wind speeds larger than 10 m s^{-1}. This trend is independent of the threshold on relative wind speed and stability. In contrast, for low wind speeds, values of the ratio are found to vary significantly with the relative wind direction. Moreover, for $U_r < 10$ m s^{-1}, the mean values in 10° bins are found to vary with the threshold on wind speed and stability. The averaged ratio for all wind direction and for wind speeds below 10 m s^{-1} is however always found to be about 1. Thus we have considered that the vertical elevations do not depend on wind direction for low wind speed and that the variations of mean values in 10° bins was due to low statistical degrees of freedom.

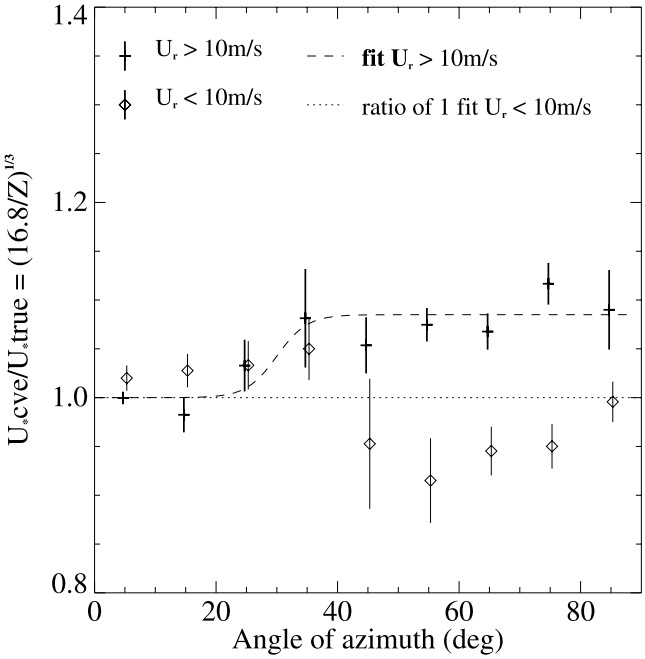

Figure 6. Mean and standard errors (standard deviation divided by the root mean square of number of samples) of the ratio of friction velocities as a function of azimuth angle at the sensor location in 10° bins. The ordinates are the mean friction velocity obtained for bow-on flows divided by the friction velocity at any relative wind direction by IDM with constant vertical elevation correction (CVE).

[38] As for the highest wind speeds, the ratio is found to increase for relative wind directions greater than about 30°, the flow is thus elevated by more than the constant value used in the "CVE" algorithm. The fit proposed for $(Z_{CVE}/Z_{true})^{1/3}$ is:

$$(Z_{CVE}/Z_{true})^{1/3} = f(\mathbf{U_r}) * 0.0425 * [\tanh((\phi_s - 30)/5) + 1] + 1 \quad (18)$$

where $f(U_r) = 0.5 * [\tanh(U_r - 10) + 1]$ is introduced to allow for a smooth transition between the two wind speed regimes (the dashed line in Figure 6 corresponds to equation (18)).

[39] Figure 7 shows the resulting vertical displacement as a function of relative wind direction for four different relative wind speeds. The maximum value of about 5 m is reached for 90° at high wind speeds. It implies that the shape of the blocking body in the stream is an important parameter. Indeed, a ship is designed to receive the sea and the wind by the stem not by the side. From the side, the shape is more vertical and the flow is significantly elevated. These results are in qualitative agreement with *Yelland et al.* [2002] results. Indeed, they obtain with three dimensional computational fluid dynamics model, vertical elevations of 1 and 5 m respectively for simulations of flows at 0 and 90° from the bow of the ship. The FETCH data on R/V *L'Atalante* suggest that the vertical elevation can be considered as constant (1.21 m from numerical simulations) up to relative wind directions of 20 or 25°. Above these angles it is also more or less constant (both data and numerical simulation) for a given wind speed. The agreement with values obtained from the numerical simulations is good; see Figure 7, where the simulation results of Table 1 are displayed with large triangles. However, the shift between bow and side values is observed at under 20° for the numerical simulations while it is at 30° for the data analysis. Also, slightly smaller values than from the data are obtained (Δz of about 2.5 and 3 m are respectively obtained for 10 m s^{-1} relative wind speed with numerical simulations and data analysis). But it should be noted that the threshold of 10 m s^{-1} to separate low and high wind speeds in the data, as well as the shape of equation (18) is somewhat arbitrary. A complete validation of the formula for the vertical elevation should take into account numerical simulations for a wider range of relative wind directions (mostly between 0 and 50°) and relative wind speeds (such as 5 and 15 m s^{-1}).

[40] Figure 8 is the similar to Figure 5b but equation (18) has been used to compute the vertical elevation using the "complete flow distortion correction". The data are now consistent for all wind speeds and directions, providing a verification that equation (18) provides a realistic estimation of the vertical displacement.

[41] In conclusion, a function for the vertical elevation is proposed for the FETCH data. It shows two regimes in relative wind directions (threshold at about 25°) and wind speeds (threshold at about 10 m s^{-1}) whose values for the higher wind speeds are in qualitative agreement with the numerical simulations at 10 m s^{-1}. A further independent analysis of the consistency of momentum flux is shown in the next section by comparing both friction velocities and mean wind speed involved in C_{D10N} values with results of the ASIS buoy.

6.2. Comparison With the ASIS Buoy Results

[42] The FETCH experiment provides the opportunity to compare two different platforms and methods in terms of

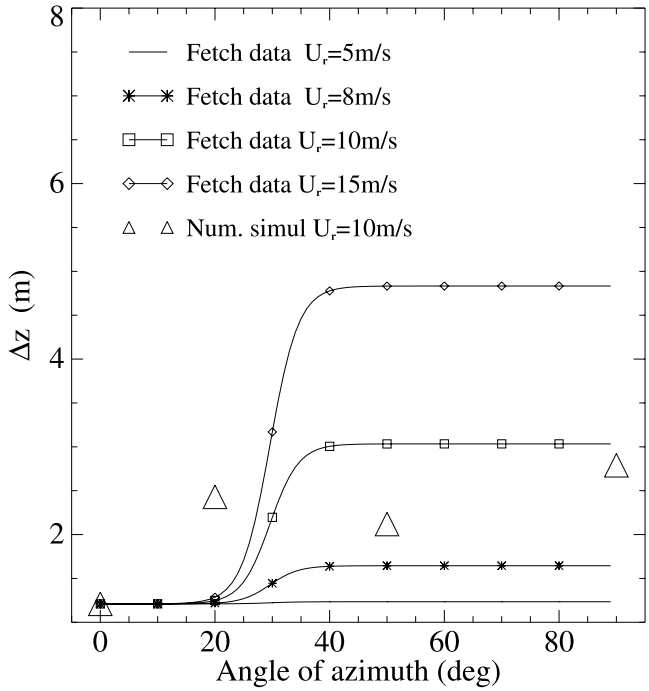

Figure 7. Comparison of vertical elevations as obtained from the FETCH data (equation (18)) and from the numerical simulations.

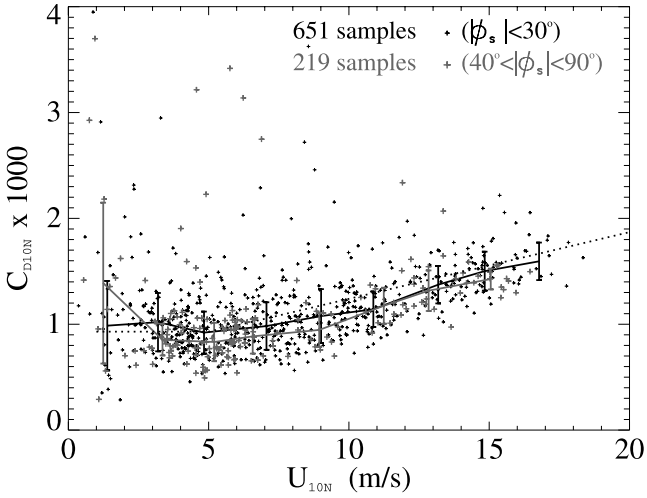

Figure 8. As in Figure 5b but using the complete airflow distortion correction, with the vertical streamline displacement given by equation (18). In this case the two ranges of relative wind direction collapse for all wind speeds.

momentum flux. However attention should be paid to effects of spatial inhomogeneities since the R/V *L'Atalante* moved in a 100 km × 100 km area while the ASIS buoy was fixed [*Hauser et al.*, 2000, 2003]. To take this into account two different thresholds, 5 and 20 km in the maximum distance between the two platforms have been selected in scatterplots of U_{10N} and u* in Figure 9 (two ranges of relative wind direction are considered, below 30° and above 40°, but it does not allow a complete study for angles above 40° since there are very few samples and they correspond to low wind speed conditions). The larger distance threshold yields larger number of samples in the comparison (66 compared to 30 for U_{10N}). The number of samples for the friction velocity comparison is slightly smaller due to a few negative $\langle -uw \rangle$ values by eddy correlation at low wind speeds: the dissipation method can yield only positive values. Figures 9a and 9c show that the flow distortion correction based on Fluent numerical simulations as described above allows a very good agreement for U_{10N} measurements between ASIS and *L'Atalante* since the regression lines are very close to the identity, although the slopes are slightly less than 1 (regression lines calculated for open symbols with relative wind directions within ±30° from the bow axis are indicated in the figures). In contrast, regression lines obtained without flow distortion corrections were instead, respectively

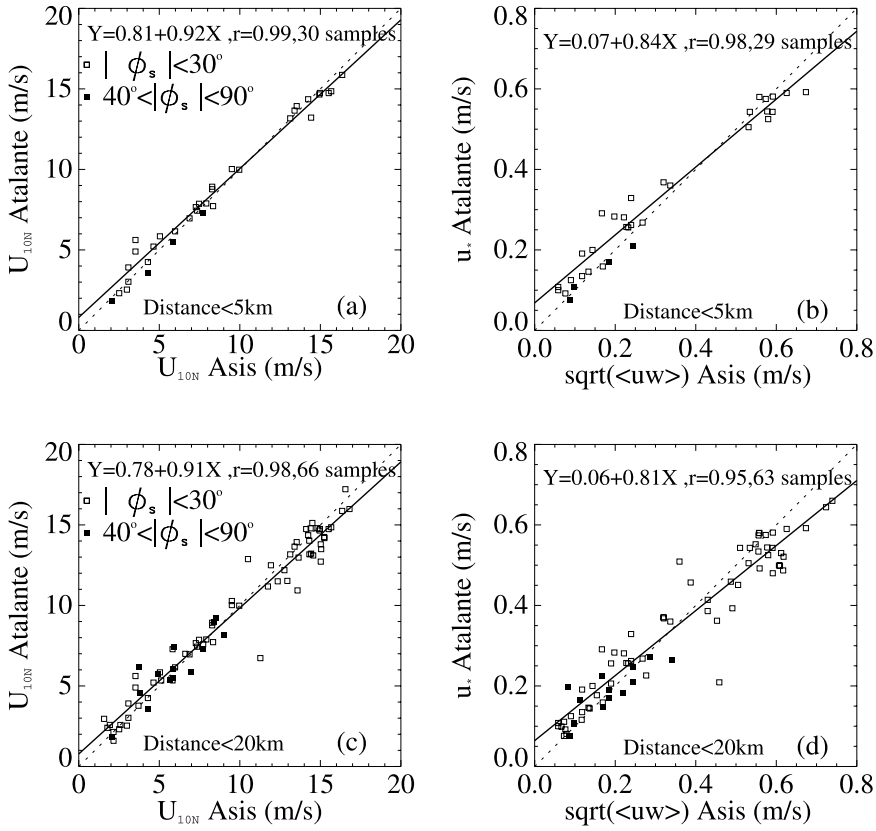

Figure 9. Comparison of the R/V *L'Atalante* and ASIS buoy (left) wind speeds and (right) friction velocities after flow distortion corrections, using two different thresholds on the maximum distance between the two platforms (5 and 20 km). The comparison is shown as a scatterplot between the ship and buoy data. Two different symbols display two ranges of relative wind direction. In Figures 9b and 9d, the momentum flux is defined as u* for the inertial dissipation method and the root mean square of $\langle -uw \rangle$ for the eddy correlation method.

for 5 and 20 km distance, y = 0.80 + 0.86x, r = 0.99 and y = 0.69 + 0.85x, r = 0.98, both associated with wind speed underestimation. The increase in the range of distance only introduces a higher scatter (correlation coefficients are 0.99 and 0.98 for the 5 and 20 km distance thresholds, respectively, in Figures 9a and 9c).

[43] In the comparison of u* by *L'Atalante* (inertial dissipation) and the root mean square of $\langle -uw \rangle$ by ASIS (Eddy Correlation), ASIS values are statistically lower (respectively higher) than those of *L'Atalante* at low (respectively high) winds (see Figures 9b and 9d). The ASIS results are those using only the along-wind component $\langle -uw \rangle$ [*Drennan et al.*, 2003]. The regression line cuts the identity line at wind speeds of about 12 m s^{-1} (or friction velocities of about 0.45 m s^{-1}). Taking the cross-wind component, $\langle -vw \rangle$, into account increases the ASIS momentum fluxes for wind speeds below 6 m s^{-1}, leading in this case to greater u* (or C_{D10N}) values than those from *L'Atalante* in the range of smooth aerodynamic flows but it has no significant effect at higher winds. Again increasing the separation distance between the two platforms increases both the scatter in the data and the numbers of samples for which the momentum flux is higher at ASIS at high winds. The regression slope remains less than 1 without the correction for distortion on the R/V *L'Atalante*. Indeed, the correction effect is mostly restricted to the vertical displacement. This correction amplifies by 3% the discrepancy for u* (for example the slope in the regression line was found to be 0.87 compared to 0.84 after corrections in Figure 9b). This value of 3% is fully explained by equation (6) showing that in the simpler case of neutral stratification, u* derived by the inertial dissipation method is proportional to $Z^{1/3}$ (an increase of 2.3% of u* is hence expected when the vertical displacement correction is applied).

[44] In summary, this comparison indicates that mean wind speeds of the R/V *L'Atalante* are well corrected for airflow distortion around the ship although the regression indicates a very slight underestimation of *L'Atalante* wind speeds compared to the buoy at high wind speeds. This suggests that the wind speed error function provided by numerical simulation is realistic. However, the correction (principally due to vertical displacement) for the *L'Atalante* fluxes does not improve their agreement with the ASIS fluxes. On the contrary, the slope of the regression between the friction velocities decreased from 0.87 to 0.84 after correction. Since horizontal distances between platforms of less than 20 km or even 5 km were considered, differences in sea state cannot be responsible for the observed flux differences. The small discrepancy is likely due to the method (dissipation versus correlation), or to sonic anemometer calibrations.

[45] Since the correction for wind speed is of higher magnitude than that for u* for bow-on flows using the inertial dissipation method (respectively about 9 and −2%), the behavior of C_{D10N} values is significantly improved by this correction, as also shown by the better self-consistency of C_{D10N} in the previous section. Since the regression lines tend to cut the identity line at wind speeds of about 12 m s^{-1}, over and under-estimates of *L'Atalante* C_{D10N} values are awaited compared to ASIS values respectively at wind speeds below and above this threshold, as will be further discussed in section 6.4 extrapolating the drag coefficient comparison to all data independently of the distance between the two platforms.

[46] In the next section, an analysis of the sensitivity of drag or exchange coefficients to simplifications in the airflow correction is described.

6.3. Effects of Flow Distortion on the Transfer Coefficients

[47] This section deals with modifications in C_{D10N}, C_{E10N} for different configurations of airflow corrections. Relative wind directions (azimuth angles) up to ±90 degrees are analyzed to discuss the modifications for different ranges of relative wind directions: ±30, ±50, ±70 and ±90°. The effect of the complete correction (subscript c) on turbulent flux parameterization is compared to the "uncorrected" parameterization (subscript u). Then, to estimate the impact of the two parts of the correction (wind vector and vertical air flow displacement) we also show results for a "wind only" flow distortion correction (subscript w), which means that correction for vertical airflow displacement is not taken into account in this case. Finally, results for a "simplified" air flow distortion correction (subscript s) are shown. In this latter case, we correct for a constant wind error affecting only the wind speed, independent of azimuth angle and we fix the vertical displacement. The values chosen in this "simplified correction" are an error of −5% on wind speed (underestimation) and a value of 1 m for the upward mean air flow displacement [*Hare et al.*, 1999].

[48] Averaged exchange coefficients C_{D10N}, C_{E10N} and C_{H10N} are presented in Table 2 for the four cases of airflow corrections and for azimuth angles within ±30° from the bow axis. The values in Table 2 are calculated as median values for 2 m s^{-1} wind speed bins. Standard deviations are displayed in parentheses below the median value.

[49] Table 2 shows that in all cases, the exchange coefficients are decreased when a correction for flow distortion is applied. It can also be noted that, for all wind speeds, applying a correction leads to a smaller standard deviation with respect to the results obtained without correction for flow distortion. The largest modifications to drag or exchange coefficients are found at high winds but the relative error is largely independent of wind speed. Tables 3 and 4 present the relative errors for C_{D10N} and C_{E10N} respectively, where the case of complete correction of flow distortion (subscript c) is taken as a reference. Results for different limits of azimuth angles (from ±30 to ±90°, every 20°) are distinguished in Tables 3 and 4. It should however be noted that the distribution of the FETCH data on the R/V *L'Atalante* is not equally distributed with respect to relative wind direction since the cruise plan called for the ship to steam into the wind when ever possible. Therefore the trends with the wind direction observed here could be stronger when applied to other datasets. Indeed, the order of magnitude of vertical displacement and wind speed error correction on C_{D10N} values are of −4.6%/−12%, −19%/0% and −19%/+40% for relative wind directions of respectively 0, 38° and 90° if high wind speeds are considered (equations (1), (2), (18)). The two corrections are in competition for angles above 38°, with the wind speed error dominating for bow-off flows; the vertical displacement effect dominates in the middle range of relative wind angles. Also, at

Table 2. C_{D10N}, C_{E10N}, and C_{H10N} Values Obtained in 2 m s^{-1} Wind Speed Bins for the Different Flow Distortion Correction Algorithms and for Azimuth Angles Within ±30°[a]

	U, m s^{-1}								
	0–2	2–4	4–6	6–8	8–10	10–12	12–14	14–16	16–18
C_{D10Nu}	1.100 (0.53)	1.113 (0.29)	1.072 (0.26)	1.180 (0.26)	1.311 (0.27)	1.459 (0.28)	1.747 (0.20)	1.939 (0.26)	2.016 (0.22)
C_{D10Nc}	0.987 (0.42)	1.020 (0.28)	0.921 (0.20)	0.983 (0.22)	1.077 (0.25)	1.141 (0.17)	1.374 (0.18)	1.502 (0.18)	1.594 (0.18)
C_{D10Nw}	0.971 (0.44)	1.070 (0.30)	0.960 (0.21)	1.039 (0.24)	1.140 (0.27)	1.205 (0.18)	1.462 (0.19)	1.600 (0.19)	1.767 (0.21)
C_{D10Ns}	1.008 (0.44)	1.010 (0.27)	0.933 (0.20)	1.018 (0.24)	1.114 (0.27)	1.179 (0.19)	1.421 (0.17)	1.559 (0.17)	1.750 (0.20)
C_{E10Nu}	1.376 (0.63)	0.912 (0.28)	0.946 (0.26)	1.045 (0.17)	1.122 (0.19)	1.155 (0.16)	1.215 (0.10)	1.235 (0.10)	1.218 (0.08)
C_{D10Nc}	1.113 (0.47)	0.817 (0.26)	0.852 (0.22)	0.911 (0.16)	0.943 (0.17)	1.015 (0.13)	1.058 (0.10)	1.069 (0.11)	1.090 (0.05)
C_{E10Nw}	1.168 (0.50)	0.873 (0.27)	0.902 (0.24)	0.968 (0.17)	1.006 (0.19)	1.069 (0.13)	1.121 (0.11)	1.136 (0.12)	1.163 (0.05)
C_{E10Ns}	1.157 (0.48)	0.822 (0.25)	0.845 (0.21)	0.939 (0.16)	0.985 (0.19)	1.015 (0.11)	1.080 (0.10)	1.098 (0.11)	1.141 (0.07)
C_{H10Nu}	1.186 (0.67)	0.927 (0.27)	1.054 (0.39)	1.359 (0.49)	1.631 (0.62)	1.504 (0.49)	2.156 (0.70)	2.045 (0.61)	2.628 (0.48)
C_{H10Nc}	0.941 (0.42)	0.830 (0.28)	0.917 (0.35)	1.134 (0.43)	1.414 (0.67)	1.316 (0.36)	1.844 (0.79)	1.679 (0.49)	1.960 (0.52)
C_{H10Nw}	1.009 (0.44)	0.911 (0.33)	0.987 (0.37)	1.228 (0.46)	1.469 (0.66)	1.416 (0.38)	2.016 (0.84)	1.779 (0.53)	2.215 (0.52)
C_{H10Ns}	0.968 (0.48)	0.812 (0.26)	0.907 (0.33)	1.187 (0.45)	1.417 (0.62)	1.321 (0.35)	1.920 (0.79)	1.698 (0.51)	2.134 (0.46)

[a]The mean values are indicated as well as standard deviations in parentheses. The air flow correction algorithms are listed as "uncorrected", subscript u; "wind only", subscript w; "simplified", subscript s; and "complete flow distortion correction", subscript c.

some wind direction, the two corrections cancel. The results of Tables 3 and 4 are a combination of these corrections applied to a particular distribution of wind speeds and directions.

[50] Concerning the C_{D10N} values, the second column of Table 3 shows that the complete airflow correction applied to the narrowest range of azimuth angles (±30°) leads to a decrease of about 17% in the C_{D10N} values. The decrease is smaller when the azimuth angle range is wider, with a minimum value of 9% for the wider range (±90°). One should keep in mind that if errors in average values of C_{D10N} without airflow distortion corrections are decreased by using a wider range of relative wind direction, this is due to the averaging of samples whose errors cancels. Thus the scatter is in this case very large and individual samples may be significantly biased.

[51] As seen in last line of column 3 in Table 3, showing the error between the full air flow distortion and the wind only correction, the vertical displacement of 1.21 m (with respect to the 17.80 m height for measurements) leads to a decrease in C_{D10N} values of 5% which is fully explained by the proportionality of u^{*2} to $Z^{2/3}$ in equation (6) mentioned above. At low azimuth angles (±30°), the vertical displacement represents about 25% of the C_{D10N} correction while 75% is due to horizontal wind speed correction which is the same order of magnitude as the values indicated above for bow angles. For larger ranges of azimuth angle, vertical displacement has a greater impact and the wind only configuration gives higher errors (−6.6% for 90° as a threshold).

[52] The error in the case of a simplified correction for air flow distortion (last columns of Table 3) is about −2% if the azimuth angles are limited to ±30° (partly due to the difference in the vertical elevation of 0.21 m at bow-on flow). Due to a cancelling of the two correction terms, the error first decreases as the flow angle range increases, finally the error reaches +4% if the azimuth angles are limited to ±90°. At these large angles, the wind speed error is overestimated (or even of the wrong sign) in the simplified correction. Again, as mentioned above for the complete correction, one should keep in mind that if, at first glance, the simplified correction may give small errors in average up to angles of 70° within the bow axis, this is only due to error cancellations. In fact this correction works properly for individual samples only for bow-on flows.

[53] Very similar trends are observed for C_{E10N} values (Table 4), although the correction for airflow distortion has less impact than on C_{D10N} values: the relative error of C_{E10N} varies from less than −13% for the smallest range of azimuth angles (±30°) to −10% in for the ±90° range. Using equations (6)–(8), we can establish that at unstable stratification, the dependence of $\langle wt_s \rangle$ or $\langle wn \rangle$ on the height of measurement follows a 5/6 power law. Therefore a relative correction of −5.7% is obtained for a vertical displacement of 1.21 m (respectively −23% for 5 m) from 17.80 m, which is similar to the value of −5.7% in Table 4. At low azimuth angles, the vertical displacement represents 45% of the total correction for the exchange coefficient for evaporation compared to 27% for the drag coefficient. Table 4, shows that the use of the simplified correction

Table 3. Comparison of Percent Errors in C_{D10N} Values Using Different Flow Distortion Correction Algorithms[a]

Azimuth Angle Limit, deg	$\left\langle \frac{C_{D10N_c} - C_{D10N_u}}{C_{D10N_c}} \right\rangle$ on Samples, %	$\left\langle \frac{C_{D10N_c} - C_{D10N_w}}{C_{D10N_c}} \right\rangle$ on Samples, %	$\left\langle \frac{C_{D10N_c} - C_{D10N_s}}{C_{D10N_c}} \right\rangle$ on Samples, %
±90 (925)	−8.9	−6.6	4.4
±70 (854)	−11.1	−6.3	2.7
±50 (755)	−14.1	−5.6	0.4
±30 (651)	−17.1	−5.0	−1.9

[a]Correction algorithms are uncorrected (subscript u), wind only (subscript w), and simplified (subscript s), using the complete flow distortion correction (subscript c) as a reference. The errors are shown as a function of azimuth angle (or relative wind direction) in degrees. The number of samples in indicated in parenthesis in the first column.

Table 4. Comparison of Percent Errors in C_{E10N} Values Using Different Flow Distortion Correction Algorithms[a]

Azimuth Angle Limit, deg	$\left\langle \frac{C_{E10N_c} - C_{E10N_u}}{C_{E10N_c}} \right\rangle$ on Samples, %	$\left\langle \frac{C_{E10N_c} - C_{E10N_w}}{C_{E10N_c}} \right\rangle$ on Samples, %	$\left\langle \frac{C_{E10N_c} - C_{E10N_s}}{C_{E10N_c}} \right\rangle$ on Samples, %
±90 (559)	−10.0	−7.2	0.3
±70 (544)	−10.4	−7.1	0.0
±50 (494)	−11.6	−6.3	−0.9
±30 (442)	−12.7	−5.7	−1.8

[a]Correction algorithms are uncorrected (subscript u), wind only (subscript w), and simplified (subscript s), using the complete flow distortion correction (subscript c) as a reference. The error is shown as a function of azimuth angle (or relative wind direction) in degrees. The number of samples in indicated in parenthesis in the first column.

leads to smaller impact on C_{E10N} values than on C_{D10N} values (1.8% maximum error compared to 4.4%).

[54] Due to the similarity of equations (7) and (8), the corrections on C_{H10N} values are very similar to those of C_{E10N} values.

6.4. Discussion of the Fetch Parameterizations

[55] Figure 10 compares drag coefficients of this study using data limited to bow-on flow (±30°) with results from the ASIS buoy (including all sea states, using only $\langle -uw \rangle$) and with those of *Smith* [1980]. Again, it clearly shows that if no correction for flow distortion is applied (gray line with error bars) an overestimation by about 15% on C_{D10N} values is obtained compared to other studies. In contrast, when the correction is applied (black heavy line with error bars), C_{D10N} values are similar to those of the ASIS buoy (thin black line with error bars) and slightly lower by a few % than those of *Smith* [1980] (dotted line). It should be noted that measurements of *Smith* [1980] were made on a platform (the Bedford Institute of Oceanography tower) which causes little airflow distortion since it was designed, like the ASIS buoy, to present very little obstruction to the air flow. *Yelland et al.* [1998] found results very similar to *Smith* [1980] after their airflow distortion (see Table 5 which compares several C_{D10N} formula) It should be noted that the results of *Anderson* [1993] and *Large and Pond* [1981], although obtained on ship-mounted instruments and not corrected for airflow distortion also compare well to *Smith* [1980]. *Yelland et al.* [1998] suggest that it could be due to cancelling effects of the dissipation function (or imbalance term) and relatively small airflow distortion (about 3% wind speed error). The relatively large range of relative wind directions used in these studies (see Table 5) should also be pointed out (see section 6.3).

[56] However, some differences are noticeable between the three curves of ASIS, R/V *L'Atalante* and *Smith* [1980], although they all collapse for U_{10N} around 13 m s^{-1}. Indeed, if the aerodynamic rough flow conditions are considered (associated with a linear trend between C_{D10N} and U_{10N}), Figure 10 indicates that the three datasets have different slopes with U_{10N}. The difference observed between *L'Atalante* and ASIS buoy C_{D10N} values is similar to what was awaited from U_{10N} and u* comparisons in section 6.2 (while the two platforms were in the vicinity of each other). Also, the threshold above which a linear trend is observed is higher for the ASIS results. Therefore the coefficients for the regressions are expressed in Table 5 using the two thresholds for U_{10N} of 6 and 8 m s^{-1}. The correlation coefficients show that only for ASIS results is the threshold of 8 m s^{-1} necessary (using the 6 m s^{-1} threshold leads to a smaller correlation coefficient and a poor fit of the regression line at high wind speeds). The slopes of other studies conducted in the open ocean mentioned in Table 5 are found to vary between 0.063 to 0.071 (first column in Table 5), whose differences are not statistically significant according to the standard errors of the slopes (the differences in the slopes are less or equal than twice the mean standard error, where the mean is the root mean square of the average of the squared standard errors). The linear regressions presented in Table 5 for the ASIS buoy (for wind speed larger than 8 m s^{-1}) and the R/V *L'Atalante* are also displayed in Figure 10 as the thin and thick lines with symbols. The slopes of the present study with R/V *L'Atalante* data are within the range of previous estimates, while the ASIS results provide a higher slope of 0.100. In this case, the difference in the slope is statistically significant. If, however, the slope is calculated over the wider wind speed range used by Smith (U > 6 m s^{-1}), the slope of the ASIS data drops to 0.77. Corresponding differences between the C_{D10N} values of

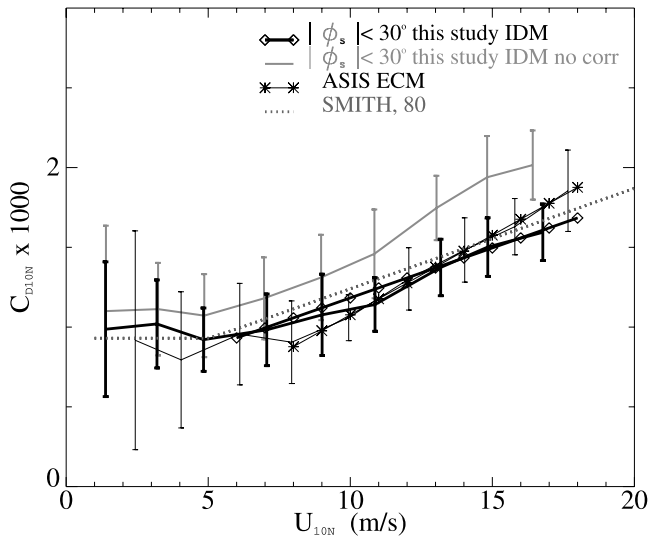

Figure 10. C_{D10N} versus U_{10N} relationships obtained during FETCH from the R/V *L'Atalante* observations with the inertial dissipation method and from the ASIS buoy using the eddy correlation method. For the FETCH results, lines with error bars show the average and standard deviation of C_{D10N} values in 2 m s^{-1} wind speed bins, whereas the lines with symbols are the regression curves given in Table 5 for wind speeds above 6 and 8 m s^{-1} for the *L'Atalante* and ASIS, respectively. The *Smith* [1980] relationship is shown as the dotted line.

Table 5. Drag Coefficient Relationships Obtained in Previous Open Ocean Studies[a]

Study	a (Slope)	b (Constant)	r	Range in U_{10N}, m s^{-1}	Data (Length)	Relative Wind Direction
Smith [1980]	0.063	0.61	0.70	6–22	63	N/A
Large and Pond [1981]	0.065	0.49	0.74	10–26	973	−90 to +45°
Large and Pond [1981]	0	1.14		4–10	618	−90 to +45°
Anderson [1993] IDM	0.071	0.49	0.91	4.5–18	84	−45 to 45°
Anderson [1993] IDM	0.065	0.59	0.83	10–18	61	−45 to 45°
Yelland et al. [1998] IDM	0.070 (0.002)	0.50 (0.02)	0.80	6–25	1111 (10)	−10 to +10°
ASIS/FETCH ECM	0.077 (0.004)	0.38 (0.04)	0.67	6–20	524	−30 to +30°
ASIS/FETCH ECM	0.100 (0.004)	0.08 (0.05)	0.77	8–20	346	−30 to +30°
This study IDM	0.063 (0.005)	0.56 (0.05)	0.56	6–19	395	−30 to +30°
This study IDM	0.069 (0.005)	0.47 (0.07)	0.54	8–19	291	−30 to +30°

[a]In each case, the formulae quoted were of the form 1000 C_{D10N} = a U_{10N} + b by linear regression (the standard errors of a and b are indicated in parentheses when available). The regression coefficients, the wind speed and direction ranges, and the number of samples used in each study are indicated.

the R/V *L'Atalante* and *Smith* [1980] are all within 6% (the maximum of 6% is obtained for 8 m s^{-1}). Maximum differences between the C_{D10N} values of ASIS and *Smith* [1980] are −18% at 8 m s^{-1} and +8% at 17.80 m s^{-1}.

[57] *Drennan et al.* [this issue] associate these differences with a wave age effect. Considering the subset of FETCH data representing pure wind seas, the high wind speed ASIS data were found to be representative of young, underdeveloped waves. The *Smith* [1980] curve, on the other hand, was found to represent near fully developed seas. With this in mind, a preliminary study has been done to compare wave age as U_{10N}/Cp both on the R/V *L'Atalante* and ASIS buoy during FETCH in the 8–18 m s^{-1} wind speed range (corresponding to rough flows and sea states dominated by wind seas). Here Cp represents the phase speed of waves at the peak of spectrum. The preliminary results, based on wave ages estimated using the VAG model [*Guillaume*, 1990], did not indicate a sea state effect with the *L'Atalante* data sufficient to account for the differences in C_{D10N} values which is supported by the similar trends obtained in section 6.2 while the two platforms encountered similar sea states; further analysis will be undertaken also to consider the controversy about use of IDM in high wind conditions [*Janssen*, 1999; *Taylor and Yelland*, 2000], indicating that this question is still unresolved. As pointed out above, accounting for the cross wind component $\langle -vw \rangle$ in the wind stress of the ASIS buoy data does not change significantly the drag coefficient for rough flow conditions. In contrast data for low and moderate wind speeds, the ASIS drag coefficients are increased after including this term.

[58] Results for the heat fluxes are shown in Figure 11. The confidence in C_{H10N} is very low (very large standard deviations compared to any other kind of measurements as also shown in Table 2). These large standard deviations are partly due to rather small air-sea temperature differences during FETCH, although air-sea temperature differences less than 0.5°C in magnitude have been excluded of the present analysis. In addition, although we have tried to use the lowest frequency part of the inertial sub-range for the sonic temperature, systematic errors due to the poor quality of the spectra also affect the order of magnitude of the sensible heat flux. It is therefore difficult to draw conclusions either on the order of magnitude of C_{H10N} values, or on the dependence of C_{H10N} values on U_{10N}.

[59] In contrast, the C_{E10N} values do not show this large scatter thanks to the refractometer measurements which

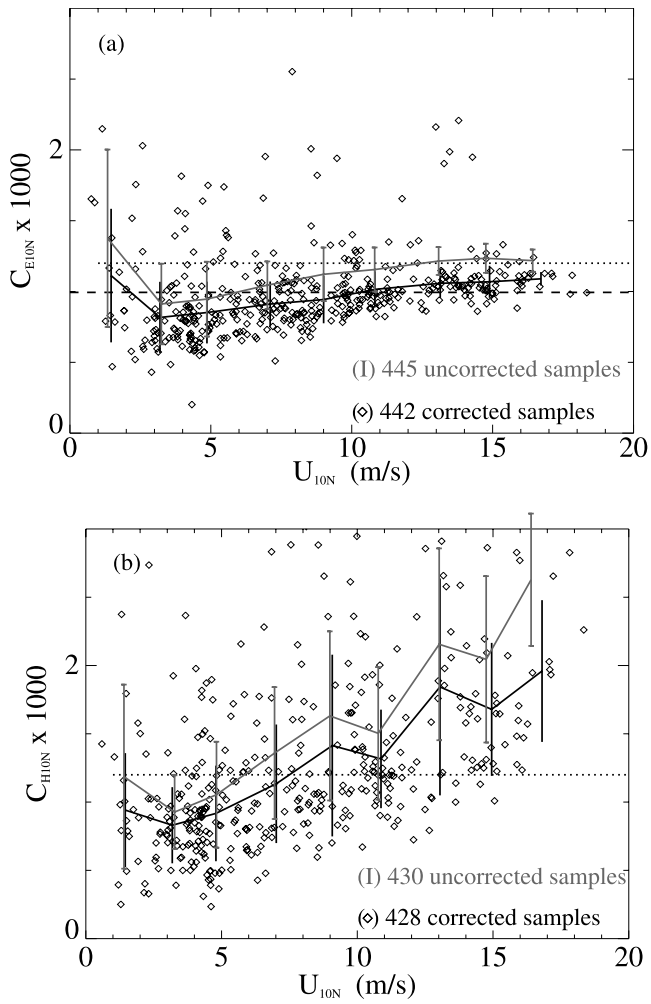

Figure 11. C_{E10N} (a) and C_{H10N} (b) versus U_{10N} obtained during FETCH from the R/V *L'Atalante* observations with the inertial dissipation method. The azimuth angles are limited to ±30° and the cases for "complete" (diamonds and solid line with error bars) and "uncorrected" (shaded line with error bars) airflow distortion corrections are displayed. Error bars are shown within 2 m s^{-1} bins in wind speed. The average value is displayed with dashed line and the 1.2 × 10^{-3} value with the dotted line.

provide refraction index fluctuation spectra with a high accuracy. The average value and standard deviations of C_{E10N} values are respectively 1.00×10^{-3} and 0.31×10^{-3} (480 samples). This compares reasonably well with previous studies by *DeCosmo et al.* [1996], *Anderson*, [1993], *Smith* [1980], and *Large and Pond* [1982], reporting values between 1 and 1.2×10^{-3} although it is slightly lower on average, especially at moderate wind speeds. The standard deviations are very small compared to previously mentioned studies. This is very encouraging for latent heat fluxes provided by these new refractometer devices. A slight dependence of C_{E10N} values with U_{10N} is observed both with or without flow distortion correction as reported by *Dupuis et al.* [1999]. This slight dependence on U_{10N} (20% within a 10 m s^{-1} wind speed range) is expressed by the following regression line (showing uncertainties of 2 standard errors):

$$C_{E10N} \times 1000 = 0.02(\pm 0.05)U_{10N} + 0.83(\pm 0.054), \quad r = 0.22(290 \text{ samples}) \tag{19}$$

[60] The remaining uncertainties due to the limit of the simulation of air flow distortion does not allow us to conclude whether this slight linear trend is real.

7. Conclusions

[61] This study concerns the estimation and parameterization of the turbulent fluxes of momentum, sensible heat and latent heat. Results were obtained by using the inertial dissipation method on the R/V *L'Atalante* during the FETCH experiment. Momentum and latent heat flux derived from a sonic anemometer and a refractometer are of good quality whereas the sensible heat flux derived from the sound speed provided by the sonic anemometer is doubtful (due to spikes in the spectra, noise limiting the inertial subrange, and also very small air-sea temperature differences leading to large standard deviations in the C_{H10N}).

[62] The main objective of the present study was to analyze the impact of airflow distortion due to the ship structure on the flux parameterizations. Therefore numerical simulations of the flow around the ship structure have been performed [*Nacass*, 1999]. They provide numerical estimates of the wind speed error, of the relative wind direction error and of the streamline slope angle as a function of the azimuth angle.

[63] These numerical simulations show a constant slope angle of about 7° for relative wind direction within ±100°. The horizontal wind speed error is found to vary from −6% to 0 to +20% for relative wind directions of respectively 0, 38 and 100°. Comparisons of simulated streamline slope angles with those measured at the sonic anemometer location show good agreement. A good agreement is found also with physical simulations realized by *Butet* [2002].

[64] Estimate of the vertical elevation of the streamline is cruder, due to the discretization and to the limited size of the domain used in the simulation. This vertical streamline displacement was however estimated by following the reverse path line and found to be 1.21 m for bow-on flows at 10 m s^{-1}. A complete expression for the vertical displacement as a function of the relative wind speed and direction (equation (18)) has been established by requiring consistency of the data for different relative wind directions, in qualitative agreement with the results of the numerical simulations obtained only at wind speeds of 10 m s^{-1}.

[65] As a result of combined effects of horizontal mean wind error and vertical displacement correction, the drag coefficients C_{D10N} are found to be almost independent of wind direction conditions, whereas a discrepancy of a factor of 2 was found without applying the correction. For wind directions aligned within ±30° of the bow axis, the correction of C_{D10N} values is in average −17%, divided into −12% for the wind speed correction and −5% for the vertical elevation correction. For heat flux, the relative effect of the vertical elevation correction on exchange coefficients is slightly larger, reaching −5.7%, while the wind speed correction reaches −7.%. A simplified correction independent of azimuth angles as used by *Hare et al.* [1999] has been tested. Consistent with the high sensitivity on azimuth angles in the wind speed error found by the simulations, this simplified correction is found to apply only for data with wind directions aligned within ±30° of the bow; otherwise if, for example a range of ±90° is used for azimuth angles, the error in C_{D10N} values reaches 4.4%.

[66] These results therefore show how this flow correction is needed. The comparison of wind speeds and momentum fluxes between estimates from the R/V *L'Atalante* and from the ASIS buoy when they were closer than 20 km, shows that the wind speeds are in good agreement when the flow distortion correction is applied. Furthermore, the agreement for the parameterization of the drag coefficients with other studies in the open ocean and with the ASIS buoy for rough flow is satisfactory. This was not the case when no correction for airflow distortion was applied. However, although similar values are observed around 13 m s^{-1} for the R/V *L'Atalante*, ASIS and *Smith et al.* [1980], the slopes of the linear regressions are rather different.

[67] The slightly higher momentum fluxes observed at ASIS compared to those from the R/V *L'Atalante* when they were in the vicinity during the FETCH cruise, as well as the different C_{D10N} values for the overall datasets at high wind speeds is one point which is not yet fully explained. Because measurements on ASIS and the R/V *L'Atalante* were obtained with two different methods, it is still difficult to draw any conclusions but this study has shown that the air flow distortion correction removes much of the discrepancies between bow-on and beam-on C_{D10N} data, yielding reasonable C_{D10N} to U_{10N} relationship and reducing the scatter (Table 2).

[68] The exchange coefficient for evaporation exhibits a very slight dependence on wind speed. Further measurements, particularly at very high wind speeds, and an enhanced confidence in the flow correction algorithm (particularly on the vertical displacement), will be needed to establish if this dependence is significant or if the average value of 1.00×10^{-3} is to be used.

[69] Results on the exchange coefficient for sensible heat flux show that a better quality of sonic temperature measurement is needed for an accurate estimation of the sensible heat flux or exchange coefficient using the inertial dissipation method. It is hoped that the improved sonic thermometer developed by Gill Instr. in the framework of the

"Autoflux" European Community Program [*Larsen et al.*, 2000] will fulfill this requirement.

[70] **Acknowledgments.** The FETCH experiment was supported by INSU-CNRS (PATOM grants), IFREMER, the European Community (grant CEE MAS3.CT96.0051) and Météo-France. The authors wish to acknowledge the technical teams from CETP, Météo-France (France), RSMAS (USA) and NWRI (Canada) for their help with the data acquisition, as well as the officers and crew of the R/V *L'Atalante*. This is contribution 1480 of the UMR 58 05 EPOC.

References

Anderson, R. J., A study of wind stress and heat flux over the open ocean by inertial dissipation method, *J. Phys. Oceanogr.*, *23*(10), 2153–2161, 1993.

Blanc, T. V., Superstructure flow distortion corrections for wind speed and direction measurements made from Tarawa Class (LHA1–LHA5) ships, *NRL Rep. 9005*, 20 pp., Naval Res. Lab., Washington, D.C., 1986.

Blanc, T. V., Superstructure flow distortion corrections for wind speed and direction measurements made from Virginia Class (CGN38–CGN41) ships, *NRL Rep. 9026*, 24 pp., Naval Res. Lab., Washington, D.C., 1987.

Butet, A., Simulation du vent autour du N.O. Thalassa, *Note de Travail Groupe de Météorologie Expérimentale et Instrumentale 23*, Cent. Natl. de Rech. Météorol., Météo-France, Paris, Feb. 2001.

Butet, A., Simulation du vent autour du N.O. Atalante, *Note CNRM/GMEI 24*, Cent. Natl. de Rech. Météorol., Météo-France, Paris, March 2002.

Castro, I. P., and A. G. Robins, The flow around a surface-mounted cube in uniform and turbulent streams, *J. Fluid Mech.*, *79*, 307–335, 1977.

Ching, J. K. S., Ship's influence on wind measurements determined from BOMEX mast and boom data, *J. Appl. Meteorol.*, *15*(1), 102–106, 1976.

DeCosmo, J., K. B. Katsaros, S. D. Smith, R. J. Anderson, W. A. Oost, K. Bumke, and H. Chadwick, Air sea exchange of sensible heat and water vapor: The HEXOS results, *J. Geophys. Res.*, *101*, 12,001–12,016, 1996.

Delahaye, J. Y., and C. Fournet-Fayas, Appareil de mesure de la fréquence de résonance d'une cavité hyperfréquence, French Patent 88-10127, Inst. National de la Propriete Indust., Paris, 1988.

Delahaye, J. Y., C. Guérin, J. P. Vinson, H. Dupuis, A. Weill, H. Branger, L. Eymard, J. Lavergnat, and G. Lachaud, A new shipborne microwave refractometer for estimating the evaporation flux at the sea surface, *J. Atmos. Oceanic Technol.*, *18*, 459–475, 2001.

Donelan, M. A., W. M. Drennan, and K. B. Katsaros, The air-sea momentum flux in conditions of wind sea and swell, *J. Phys. Oceanogr.*, *27*(10), 1997.

Drennan, W. M., H. C. Graber, D. Hauser, and C. Quentin, On the wave age dependence of wind stress over pure wind seas, *J. Geophys. Res.*, *108*, doi:10.1029/2000JC000715, in press, 2003.

Dupuis, H., P. K. Taylor, A. Weill, and K. B. Katsaros, The inertial dissipation method applied to derive momentum fluxes over the ocean during the SOFIA/ASTEX and SEMAPHORE experiments with low to moderate wind speeds, *J. Geophys. Res.*, *102*, 21,115–21,129, 1997.

Dupuis, H., C. Guérin, A. Weill, and D. Hauser, Heat fluxes by the inertial dissipation method during FETCH, in *The Wind-Driven AIR-SEA Interface: Electro-Magnetic and Acoustic Sensing, Wave Dynamics and Turbulent Fluxes*, edited by M. Banner, pp. 297–304, Sch. of Math., Univ. of New South Wales, Sydney, Australia, 1999.

Edson, J. B., C. W. Fairall, P. G. Mestayer, and S. E. Larsen, A study of the inertial dissipation method for computing air-sea fluxes, *J. Geophys. Res.*, *96*, 10,689–10,711, 1991.

Edson, J. B., A. A. Hinton, K. E. Prada, J. E. Hare, and C. W. Fairall, Direct covariance flux estimates from mobile Platforms at sea, *J. Atmos. Oceanic Technol.*, *15*, 547–562, 1998.

Eymard, L., et al., Surface fluxes in the North Atlantic Current during the CATCH/FASTEX experiment, *Q. J. R. Meteorol. Soc.*, *125*, 3563–3599, 1999.

Fairall, C. W., and S. E. Larsen, Inertial dissipation methods and turbulent fluxes at the air-ocean interface, *Boundary Layer Meteorol.*, *34*, 287–301, 1986.

Fujitani, T., Direct measurements of turbulent fluxes over the sea during AMTEX, *Meteorol. Geophys.*, *32*, 119–134, 1981.

Geernaert, G. L., K. B. Katsaros, and K. Richter, Variations of the drag coefficient and its dependence on sea state, *J. Geophys. Res.*, *91*, 7667–7679, 1986.

Graber, H. C., E. A. Terray, M. A. Donelan, W. M. Drennan, J. C. Van Leer, and D. B. Peters, ASIS-A new air-sea interaction Spar buoy: Design and performance at sea, *J. Atmos. Oceanic Technol.*, *17*(5), 708–720, 2000.

Guillaume, A., Statistical tests for the comparison of surface gravity wave spectra with application to model validation, *J. Atmos. Oceanic Technol.*, *7*, 552–567, 1990.

Hare, J. E., P. O. Persson, C. W. Fairall, and J. B. Edson, Behavior of Charnock's relationship for high wind conditions, paper presented at 13th Conference on Boundary Layers and Turbulence, Am. Meteorol. Soc., Dallas, Tex., 10–15 Jan. 1999.

Hauser, D., H. Dupuis, X. Durrieu de Madron, C. Estournel, C. Flamant, J. Pelon, P. Queffeulou, and J. M. Lefèvre, La campagne FETCH: Une expérience pour l'étude des échanges océan/atmosphère dans les conditions côtières du Golfe du Lion, *Meteorologie*, *8*(29), 14–31, 2000.

Hauser, D., et al., The FETCH experiment: An overview, *J. Geophys. Res.*, *108*(C3), 8053, doi:10.1029/2001JC001202, 2003.

Janssen, P. A. E. M., On the effect of ocean waves on the kinetic energy balance and consequences for the inertial dissipation technique, *J. Phys. Oceanogr.*, *29*(3), 530–534, 1999.

Kitaigorodskii, S. A., *The Physics of Air-Sea Interaction* (in Russian), Gidrometeorologicheskoe Izdatel'stvo, Leningrad, 1970. (Isr. Program for Sci. Transl., Jerusalem, 1973).

Large, W. G., and S. Pond, Open ocean momentum flux measurements in moderate to strong winds, *J. Phys. Oceanogr.*, *11*, 324–336, 1981.

Large, W. G., and S. Pond, Sensible and latent heat flux measurement over the ocean, *J. Phys. Oceanogr.*, *12*, 464–482, 1982.

Larsen, S. E., J. B. Edson, C. W. Fairall, and P. G. Mestayer, Measurements of temperature spectra by a sonic anemometer, *J. Atmos. Oceanic Technol.*, *10*, 345–354, 1993.

Larsen, S. E., et al., AUTOFLUX: An autonomous fluxpackage for measuring the air-sea flux of momentum, heat, water vapour and carbon dioxide, paper presented at EurOCEAN 2000, Eur. Comm., Hamburg, Germany, 29 Aug. to 2 Sept. 2000.

Nacass, P., Utilisation de la Modélisation des Écoulements Aérodynamiques pour l'instrumentation du Navire Océanographique *L'Atalante, Note du Cent. d'Aviation Météorol. 22*, 132 pp., Météo-France, Cent. Natl. de Rech. Météorol., Paris, 1999.

Oost, W. A., C. W. Fairall, J. B. Edson, S. D. Smith, R. J. Anderson, J. A. B. Wills, K. B. Katsaros, and J. DeCosmo, Flow distortion calculations and their application in Hexmax, *J. Atmos. Oceanic Technol.*, *11*(2), 366–386, 1994.

Smith, S. A., et al., Sea surface wind stress and drag ceofficients: The HEXOS results, *Boundary Layer Meteorol.*, *60*, 109–142, 1992.

Smith, S. D., Wind stress and heat fluxes over the ocean in gale force winds, *J. Phys. Oceanogr.*, *10*, 709–726, 1980.

Smith, S. D., Coefficients for sea surface wind stress, heat flux and wind profiles as a function of windspeed and temperature, *J. Geophys. Res.*, *93*, 15,467–15,472, 1988.

Taylor, P. K., and M. J. Yelland, A note on the apparent "imbalance" term in the turbulent kinetic energy budget, *J. Atmos. Oceanic Technol.*, *17*(1), 82–89, 2000.

Volkov, Y. A., Turbulent flux of momentum and heat in the atmospheric surface layer over a disturbed surface, *Izv. Acad. Sci. USSR Atmos. Oceanic Phys.*, *6*, 770–774, 1970.

Wyngaard, J., and O. Coté, The budgets of turbulent kinetic energy and temperature variance in the atmospheric surface layer, *J. Atmos. Sci.*, *28*, 190–201, 1971.

Yelland, M. J., and P. K. Taylor, Wind stress measurements from the open ocean, *J. Phys. Oceanogr.*, *26*, 541–558, 1996.

Yelland, M. J., B. I. Moat, P. K. Taylor, R. W. Pascal, J. Hutchings, and V. C. Cornell, Wind stress measurements from the open ocean corrected for airflow distortion by the ship, *J. Phys. Oceanogr.*, *28*, 1511–1525, 1998.

Yelland, M. J., B. I. Moat, R. W. Pascal, and D. I. Berry, CFD model estimates of the airflow over research ships and the impact on momentum flux measurements, *J. Atmos. Oceanic Technol.*, *19*(10), 1477–1499, 2002.

S. Cloché, Universite Pierre et Marie Curie, IPSL/Tour 15, 4 place Jussieu, 75252 Paris Cedex 05, France.

W. M. Drennan and H. C. Graber, Rosenstiel School of Marine and Atmospheric Science, University of Miami, Miami, FL 33149, USA.

H. Dupuis, Département de Géologie et Océanographie, UMR 58 05, Avenue des Facultés, 33 405 Talence cedex, France. (dupuis@geocean.u-bordeaux.fr)

C. Guerin, D. Hauser, and A. Weill, CETP/IPSL/CNRS, 10–12 Avenue de l'Europe, 78140Vélizy, France.

P. Nacass, Meteo-France/CNRM/Centre d'Aviation Meteorologique, Aerodrome, Batiment AMOR, 91228 Bretigny-sur-Orge, France.